Estimates of mass absorption cross sections of black carbon for filter-based absorption photometers in the Arctic

Sho Ohata[1,2,*], Tatsuhiro Mori[3,4,*], Yutaka Kondo[5,*], Sangeeta Sharma[6], Antti Hyvärinen[7], Elisabeth Andrews[8,9], Peter Tunved[10,11], Eija Asmi[7], John Backman[7], Henri Servomaa[7], Daniel Veber[6], Konstantinos Eleftheriadis[12], Stergios Vratolis[12], Radovan Krejci[10,11], Paul Zieger[10,11], Makoto Koike[3], Yugo Kanaya[13,14], Atsushi Yoshida[5], Nobuhiro Moteki[3], Yongjing Zhao[15], Yutaka Tobo[5,16], Junji Matsushita[5], and Naga Oshima[17]

[1]Institute for Space–Earth Environmental Research, Nagoya University, Nagoya, Aichi, Japan
[2]Institute for Advanced Research, Nagoya University, Nagoya, Aichi, Japan
[3]Department of Earth and Planetary Science, Graduate School of Science, The University of Tokyo, Tokyo, Japan
[4]Department of Physics, Faculty of Science Division I, Tokyo University of Science, Tokyo, Japan
[5]National Institute of Polar Research, Tachikawa, Tokyo, Japan
[6]Climate Chemistry Measurements Research/Climate Research Division, Environment and Climate Change Canada/Government of Canada
[7]Finnish Meteorological Institute, Helsinki, Finland
[8]Cooperative Institute for Research in Environmental Sciences (CIRES), University of Colorado, Boulder, CO, USA
[9]NOAA Global Monitoring Laboratory, 325 Broadway, Boulder, CO, USA
[10]Department of Environmental Science, Stockholm University, Stockholm, Sweden
[11]Bolin Centre for Climate Research, Stockholm University, Stockholm, Sweden
[12]Environmental Radioactivity Laboratory (ERL), Institute of Nuclear and Radiological Science & Technology, Energy & Safety, National Centre for Scientific Research "Demokritos", 15310 Attiki, Greece
[13]Research Institute for Global Change (RIGC), Japan Agency for Marine-Earth Science and Technology (JAMSTEC), Yokohama, Kanagawa, Japan
[14]Graduate School of Maritime Sciences, Kobe University, Kobe, Japan
[15]Air Quality Research Center, University of California, Davis, CA, USA
[16]Department of Polar Science, School of Multidisciplinary Sciences, The Graduate University for Advanced Studies, SOKENDAI, Tachikawa, Tokyo, Japan
[17]Meteorological Research Institute, Tsukuba, Japan

[*]These authors contributed equally to this work.

Correspondence to: Sho Ohata (sho.ohata@isee.nagoya-u.ac.jp)

Running title: Normalization of BC measurements by COSMOS

Abstract. Long-term measurements of atmospheric mass concentrations of black carbon (BC) are needed to investigate changes in its emission, transport, and deposition. However, depending on instrumentation, parameters related to BC such as aerosol absorption coefficient (b_{abs}) have been measured instead. Most ground-based measurements of b_{abs} in the Arctic have been made by filter-based absorption photometers, including particle soot absorption photometers (PSAP), continuous light absorption photometers (CLAP), Aethalometers, and multi-angle absorption photometers (MAAP). The measured b_{abs} can be converted to mass concentrations of BC (M_{BC}) by assuming the value of the mass absorption cross section (MAC; $M_{BC} = b_{abs}$/MAC). However, the accuracy of conversion of b_{abs} to M_{BC} has not been adequately assessed. Here, we introduce a systematic method for deriving MAC values from b_{abs} measured by these instruments and independently measured M_{BC}. In this method, M_{BC} was measured with a filter-based absorption photometer with a heated inlet (COSMOS). COSMOS-derived M_{BC} (M_{BC} (COSMOS)) is traceable to a rigorously calibrated single particle soot photometer (SP2) and the absolute accuracy of M_{BC} (COSMOS) has been demonstrated previously to be about 15 % in Asia and the Arctic. The necessary conditions for application of this method are a high correlation of the measured b_{abs} with independently measured M_{BC}, and long-term stability of the regression slope, which is denoted as MAC_{cor} (MAC derived from the correlation). In general, b_{abs}–M_{BC} (COSMOS) correlations were high (r^2 = 0.76–0.95 for hourly data) at Alert in Canada, Ny-Ålesund in Svalbard, Barrow in Alaska, Pallastunturi in Finland, and Fukue in Japan, and stable for up to 10 years. We successfully estimated MAC_{cor} values (10.8–15.1 $m^2\ g^{-1}$ at a wavelength of 550 nm for hourly data) for these instruments and these MAC_{cor} values can be used to obtain error-constrained estimates of M_{BC} from b_{abs} measured at these sites even in the past, when COSMOS measurements were not made. Because the absolute values of M_{BC} at these Arctic sites estimated by this method are consistent with each other, they are applicable to the study of spatial and temporal variation of M_{BC} in the Arctic and to evaluation of the performance of numerical model calculations.

1 Introduction

Black carbon (BC) aerosols strongly absorb solar radiation and thereby impact the radiation budget in the Arctic (Bond et al., 2013; AMAP, 2015). In addition, BC deposited on snow decreases the snow surface albedo and accelerates snowmelt (AMAP, 2015; Flanner et al., 2009). According to recent climate model calculations in the sixth phase of the Coupled Model Intercomparison Project (CMIP6; Eyring et al., 2016), BC contributes the second largest positive radiative forcing in the Arctic, after carbon dioxide (CO_2) (Oshima et al., 2020). BC is one of the short-lived climate forcers (SLCFs) and reductions of BC emissions can decrease the positive Arctic radiative forcing over much shorter timescales than can reductions of CO_2 emissions (Sand et al., 2016). Long-term measurements of mass concentrations of BC in the atmosphere (M_{BC} [µg m^{-3}]) at various locations provide fundamental data for the detection of long-term trends in M_{BC} in the Arctic that are associated with changes in BC emissions. Such M_{BC} data are also useful for validation and improvement of climate models. However, because many long-term surface instruments measure aerosol light absorption coefficient (b_{abs} [Mm^{-1}]) rather than M_{BC}, there are large uncertainties in M_{BC} estimated from the measurements of b_{abs}; these uncertainties have not been critically evaluated.

A continuous soot monitoring system called COSMOS (Kanomax, Osaka, Japan) has been developed to measure M_{BC} (Miyazaki et al., 2008; Kondo et al., 2009, 2011). This filter-based absorption photometer is equipped with an inlet that is heated to 300°C to remove non-refractory components from the aerosol phase. COSMOS M_{BC} values (M_{BC} (COSMOS)) have been compared with those measured by a single particle soot photometer (SP2; Droplet Measurement Technologies, Longmont, CO, USA; M_{BC} (SP2)), which is based on a laser-induced incandescence technique (Schwarz et al., 2006; Moteki and Kondo, 2010); simultaneous measurements in Asia and at Ny-Ålesund in Svalbard have shown that M_{BC} (SP2) and M_{BC} (COSMOS) agree to within about 10 % (Kondo et al., 2009, 2011; Ohata et al., 2019).

Long-term measurements of b_{abs} at various sites have been carried out by other types of filter-based absorption photometers, including the particle absorption soot photometer (PSAP; Radiance Research, Seattle, WA, USA), the continuous light absorption photometer (CLAP; NOAA, Boulder, CO, USA; Ogren et al., 2017), the Aethalometer (Magee Scientific, Berkeley, CA, USA), and the multi-angle absorption photometer (MAAP; Thermo Scientific, Waltham, MA, USA) (e.g., Schmeisser et al., 2018). Measurements of light-absorption and light-scattering properties of aerosols are important for constraining their interannual and seasonal variability, potential particle sources, and resulting aerosol-radiation interactions in the Earth system (Schmeisser et al., 2018; Bellouin et al., 2020). However, the accuracy and stability of conversion of b_{abs} obtained by these instruments to M_{BC} have not yet been fully evaluated, mainly because of a lack of simultaneous and reliable long-term M_{BC} measurements. The relationship between b_{abs} obtained by these instruments and M_{BC} are complicated by complex contributions from mixing states of BC (i.e., lensing effect by BC-coating materials; Bond et al., 2006: Lack et al., 2008), other co-existing light-absorbing aerosols such as brown carbon and mineral dust, and measurement artifacts by light-scattering aerosols on filters (Bond et al., 1999). Evaluations that have been completed to date include those of Kanaya et al. (2013, 2020), who compared M_{BC} (COSMOS) with the b_{abs} measured by MAAP (b_{abs} (MAAP)) on Fukue Island, Japan, and Sinha et al. (2017), who compared b_{abs} measured by PSAP (b_{abs} (PSAP)) at Barrow in Alaska and Ny-Ålesund (Zeppelin station), Svalbard. The results of these studies showed that b_{abs} (MAAP) and b_{abs} (PSAP) were strongly correlated with M_{BC} (COSMOS), making it possible to convert b_{abs} to M_{BC} at these sites with reasonable accuracy. Long-term observations of b_{abs} have been made also at Arctic: Alert in Canada by PSAP and Aethalometer (Sharma et al., 2004, 2006, 2017), Ny-Ålesund by Aethalometer (Eleftheriadis et al., 2009) and MAAP, and Pallastunturi in Finland by MAAP (Hyvärinen et al., 2011; Lihavainen et al., 2015). To investigate the possibility of converting b_{abs} to M_{BC} at each of these sites, it is important to simultaneously measure M_{BC} and b_{abs} by collocating a COSMOS (or SP2) at each site with each of these filter-based absorption photometer instruments.

The conversion of b_{abs} obtained by these instruments to M_{BC} can be made by assuming a reasonable conversion factor, i.e, the value of mass absorption cross section (MAC [m^2 g^{-1}]; $M_{BC} = b_{abs}$/MAC). The MAC values can depend on location because the spatiotemporal variations in microphysical properties of BC (i.e., mixing states and size distributions) and properties of co-existing light-absorbing and scattering aerosols will affect b_{abs} measurements. The plausible MAC values for conversion can also depend on the type of instrument because each instrument uses a different wavelength or wavelengths and adopts various correction methods for quantifying b_{abs}. Despite several intercomparisons and field experiments (Asmi et al., 2020) as well as thorough assessment of these techniques (Lack et al., 2008; Moosmüller et al., 2009) the simultaneous changes in aerosol source region, mixing state, concentration and particle optical size are reflected in the instruments' response in a complex way and with a variable level of uncertainty.

In general, the MAC of BC, here simply denoted as "MAC_{BC}" for both bare and internally-mixed BC, is a fundamental optical parameter that relates M_{BC} with b_{abs} of BC ($b_{abs,BC}$) in climate models (i.e., $b_{abs,BC} = M_{BC} \times MAC_{BC}$). Bond and Bergstrom (2006) reported the MAC_{BC} value of 7.5 m^2 g^{-1} at a wavelength of 550 nm for combusted fresh BC. Cho et al., (2021) estimated MAC_{BC} values of 6–12 m^2 g^{-1} at 550 nm in the Asian outflow using aircraft-based SP2 data and Mie theory. Yuan et al. (2021) showed that the MAC_{BC} values at 870 nm at a rural site in Germany clearly increased as the coating thickness of BC increased.

However, in this paper we focus on the MAC values mainly from the viewpoint of a conversion factor to obtain error-constrained M_{BC} from the b_{abs} measurements by the filter-based absorption photometers because such M_{BC} data will be the observational base for understanding long-term trends and spatial distributions of BC in the Arctic. Detailed investigations of the accuracy of the absolute values of b_{abs} measured at each site are beyond the scope of this study.

We critically re-examine the concepts underpinning the use of filter-based instruments to estimate M_{BC}. We derive MAC values for PSAP/CLAP, Aethalometer, and MAAP measurements based on their comparison with COSMOS measurements at the four above-mentioned Arctic sites (Alert, Ny-Ålesund, Barrow, and Pallastunturi) and one East Asian site (Fukue). The variability of the derived MAC values and their dependencies on observation site and instrument type are analyzed. We also compare M_{BC} values measured by COSMOS and SP2 at Alert and Fukue to confirm their agreement under different environmental conditions.

2 Methods

2.1 Observation sites

Measurements of b_{abs} by the various types of filter-based absorption photometers were compared with measurements of M_{BC} by COSMOS at Arctic sites Alert in Canada (82.5º N, 62.5º W; Sharma et al., 2017), Ny-Ålesund (Zeppelin station) in Svalbard (78.9º N, 11.9º E; Sinha et al., 2017), Barrow in Alaska (71.3º N, 156.6º W; Sinha et al., 2017), and Pallastunturi (Pallas, hereafter) in Finland (68.0º N, 24.0º E; Hyvärinen et al., 2011), as summarized in Table 1 and Fig. 1. Along with these sites, comparisons were also made at a remote site on Fukue Island (32.8º N, 128.7º E; Kanaya et al., 2020) in Japan, where air masses from the Asian continent are occasionally transported to the site and properties of aerosols should be distinctly different from those at the Arctic sites. Instruments used at each site are listed in Table 1 and described in the following section.

2.2 Instruments

2.2.1 SP2

In this study we used the SP2 and COSMOS as standard instruments to measure M_{BC}. Detailed descriptions of the SP2, including calibration methods, are given elsewhere (Schwarz et al., 2006; Moteki and Kondo, 2010). Briefly, the SP2 uses the laser-induced incandescence technique and detects BC on a single-particle basis. We used two SP2s in this study: the one installed at Fukue was maintained and calibrated by the University of Tokyo (UT-SP2, hereafter) and the other one at Alert was maintained and calibrated by Environmental and Climate Change Canada (EC-SP2, hereafter). The configuration of the UT-SP2 is identical to that described by Moteki and Kondo (2010). The model designation of the EC-SP2 was "SP2-D" with eight channels. The UT-SP2 and EC-SP2 measured BC size distributions in the mass-equivalent diameter (D_m) range 70–850 and 60–600 nm, respectively. The void-free density of BC was assumed to be 1.8 g cm^{-3}. These SP2s were calibrated using fullerene soot particles (Alfa Aeser, stock #40971, lot #FS12S011; Moteki and Kondo, 2010; Kondo et al., 2011). The laser-induced incandescence signal intensity of the UT-SP2 for the specific mass of ambient BC particles in Tokyo agree with that of fullerene soot particles to within about 10 % (Kondo et al., 2011). Laborde et al. (2012) reported similar SP2 calibration curves for fullerene soot particles, diesel exhaust, and ambient BC particles in Switzerland. The accuracy of M_{BC} (SP2) estimated from the uncertainty of the calibration and operational conditions of SP2 was about 10 %. No particle-size cut was used for the inlet of the UT-SP2, whereas a PM_1 cyclone was used for the EC-SP2.

2.2.2 COSMOS

2.2.2.1 Measurements of M_{BC} by COSMOS

The principles of operation of the COSMOS apparatus are detailed in previous papers (Miyazaki et al., 2008; Kondo et al., 2011; Kondo, 2015; Ohata et al., 2019). Briefly, the COSMOS measures the attenuation coefficient (b_0) of aerosols collected on a quartz-fiber filter at a given wavelength (λ = 565 nm). Most previous studies used filters from Pallflex (E70-2075W, Pall, Port Washington, NY, USA), which are no longer available. Consequently, high-efficiency particulate air (HEPA) filters (L-371M) have been used for more recent observations (Irwin et al., 2015), including this study. An important difference between the COSMOS and the other types of filter-based absorption photometer is that the inlet of the COSMOS is heated to 300°C to remove volatile light scattering particles (LSPs) and coatings of BC from the aerosol phase. Therefore, the effect on b_0 of co-existing volatile components externally or internally mixed with BC particles can be ignored. The COSMOS is equipped with a PM_1 cyclone to minimize the effect in coarse mode of refractory non-BC particles, such as dust and sea-salt particles. Consequently, the absorption coefficient for the COSMOS is given as

$$b_{abs}\,(\mathrm{COSMOS}) = f_{fil} b_0. \qquad (1)$$

Here, f_{fil} is a factor used to correct for the increase of absorption caused by multiple scattering in the filter medium. It is given by

$$f_{fil}\,(Tr) = \frac{1}{[1.0796\,Tr + 0.71]\,B} \text{ with } Tr \geq 0.7, \qquad (2)$$

where Tr is the filter transmission and B is a scaling factor (Bond et al. 1999; Ogren 2010; Ohata et al., 2019). The MAC for the COSMOS [$m^2\ g^{-1}$] is operationally defined as

$$\mathrm{MAC}\,(\mathrm{COSMOS, SP2}) \equiv \frac{b_{abs}\,(\mathrm{COSMOS})}{M_{BC}\,(\mathrm{SP2})}, \qquad (3)$$

where the numerator and denominator, respectively, are simultaneous measurements of b_{abs} [Mm^{-1}] by COSMOS and M_{BC} [$\mu g\ m^{-3}$] by SP2 for ambient air. The MAC value for a Pallflex filter at λ = 565 nm was previously set at 8.73 [$m^2\ g^{-1}$] with B = 1.397 (Sinha et al., 2017). For a HEPA filter, the value of B

is about 6 % lower (Irwin et al., 2015). Depending on the filters used (Pallflex or HEPA), the appropriate B value was used in this study.

Once the MAC (COSMOS, SP2) is determined, M_{BC} (COSMOS) [g m^{-3}] at standard temperature and pressure (0°C, 1013 hPa) can be estimated as

$$M_{BC}\,(\mathrm{COSMOS}) = \frac{b_{abs}\,(\mathrm{COSMOS})}{\mathrm{MAC}\,(\mathrm{COSMOS,SP2})}. \qquad (4)$$

One particular purpose of the heating of sampled air to 300°C is to make the MAC (COSMOS, SP2) stable and independent of original mixing states of BC particles. In other words, the heating treatment makes b_{abs} (COSMOS) more proportional to BC mass concentrations, as compared to the other filter-based absorption photometers described in Sect. 2.2.3. As a consequence, unlike the other filter-based absorption photometers, the absorption coefficient of unheated original aerosols is not provided by COSMOS. Thus, the COSMOS has been developed to measure M_{BC}, not b_{abs}. In this sense, M_{BC} (COSMOS) is different from "equivalent" BC mass concentrations estimated from the unheated b_{abs} measurements (Petzold et al., 2013).

We call the COSMOS that was calibrated by comparison with the SP2 in Tokyo the "standard COSMOS", described hereafter as Std-COSMOS. Because the MAC of the Std-COSMOS was determined by comparison with SP2 (Eq. (2)), it acts as a transfer standard for the SP2. The b_{abs} (COSMOS) of each COSMOS manufactured is compared with the Std-COSMOS by sampling ambient BC particles in Osaka, Japan, typically for 1–2 weeks. The comparisons during these periods were statistically reliable partly due to relatively high BC concentrations in Osaka. The b_{abs} (COSMOS) of 28 COSMOS instruments manufactured thus far agree with that of Std-COSMOS to within about ±7 %, indicating reliable quality control in manufacturing. The small differences originating from the uncertainty of the filter sampling spot size of each unit are corrected for in deriving M_{BC} (COSMOS).

It is important to compare M_{BC} (COSMOS) and M_{BC} (SP2) outside Tokyo and Osaka, to confirm both the strong correlation between M_{BC} (COSMOS) and M_{BC} (SP2) and the long-term stability of the MAC (COSMOS) value. Ohata et al. (2019) made these comparisons at two remote sites: at Cape Hedo (26.9°N, 128.3°E), Japan, and at Ny-Ålesund. At each of these locations, the concentrations of BC and LSP and the mixing states of BC were considerably different from those in Tokyo and Osaka. M_{BC} (COSMOS) and M_{BC} (SP2) agree to within about 10 % at these sites, thus demonstrating the validity of using the Std-COSMOS to calibrate each of the COSMOS instruments to be used for field observations. Ohata et al. (2019) also showed that the dependencies of MAC (COSMOS) on the thickness of coatings of BC particles, M_{BC}, and volume concentrations of the co-existing LSPs were small. Although the MAC (COSMOS) showed a slight dependence on the mass size distributions of BC, the sensitivity of the MAC (COSMOS) to such variations in microphysical properties of BC was generally less than 10 % (Kondo et al., 2011; Ohata et al., 2019).

Previously estimated uncertainties of M_{BC} (COSMOS) were about 10 % based on the range of agreement between M_{BC} measurements by COSMOS and UT-SP2 (Kondo et al., 2011; Ohata et al., 2019). It may be more appropriate to estimate the absolute accuracy of M_{BC} (COSMOS) to be about 15 %, including the above-mentioned 10 % uncertainty of M_{BC} (SP2). This 15 % uncertainty also covers the range of agreement between M_{BC} (COSMOS) and M_{BC} (SP2) previously reported by other groups at Ny-Ålesund (Zannata et al., 2018) and at Fukue (Miyakawa et al., 2017).

Although we used the SP2 and COSMOS as standard instruments to measure M_{BC} in this study, thermal-optical analysis, which quantifies elemental carbon (EC) mass concentrations (M_{EC}), also has been a traditional standard method to measure BC. Measurements of M_{EC} can depend on the temperature protocol and optical charring correction method used (e.g., Bond et al., 2013). Agreements within 10 % of M_{BC} (SP2), M_{BC} (COSMOS), and M_{EC} were reported by Kondo et al. (2011), whereas systematic differences between M_{BC} (SP2) and M_{EC} up to a factor of 2 were found by Pileci et al. (2021). Although the difference between M_{BC} (COSMOS) and M_{EC} was generally lower than 5 ng m^{-3} at the Arctic site Barrow (Sinha et al., 2017), this difference can be important for pristine summer Arctic conditions (M_{BC} (COSMOS) < 20 ng m^{-3}). Considering these previously reported agreements and discrepancies between M_{BC} (SP2 or COSMOS) and M_{EC}, in some cases the MAC values determined by b_{abs} and M_{BC} measurements (this study) can differ from those determined by b_{abs} and M_{EC} measurements (Zanatta et al., 2016).

2.2.2.2 Effect of light-absorbing FeO_x particles on M_{BC} (COSMOS)

Light-absorbing iron oxide (FeO_x) aerosols such as magnetite, which the SP2 can distinguish from BC (Yoshida et al., 2016; Lamb, 2019), can affect M_{BC} measured by filter-based absorption photometers. FeO_x aerosols are emitted from both anthropogenic sources (e.g., motor vehicle exhaust) and natural sources (e.g., wind-blown mineral dust). Within the detectable diameter range of the UT-SP2 (D_m = 70–850 nm for BC and D_m =170–2100 nm for FeO_x), the mass concentration ratios of FeO_x to BC were typically ~0.4 in East Asia and ~0.2 in the Arctic; they were mainly of anthropogenic origin in the form of aggregated magnetite nanoparticles in both regions (Moteki et al., 2017; Ohata et al., 2018; Yoshida et al., 2018, 2020). FeO_x aerosols contribute at least 4–7 % of the short-wave absorbing powers of BC in Asian continental outflows (Moteki et al., 2017) and their direct radiative forcing has been estimated to be 0.22 W m^{-2} over East Asia (Matsui et al., 2018). Here, we estimate the effect of light absorption by FeO_x on M_{BC} measured by the COSMOS. The ratio of light absorbed by FeO_x to that absorbed by BC at a wavelength λ (ε(λ)) is given by

$$\varepsilon(\lambda) = \frac{\int_{D_L}^{D_U} \frac{dM_{FeOx}}{d\log D_m} \mathrm{MAC}_{Mie\_FeOx}(D_m,\lambda)\, d\log D_m}{\int_{D_L}^{D_U} \frac{dM_{BC}}{d\log D_m} \mathrm{MAC}_{Mie\_BC}(D_m,\lambda)\, d\log D_m}, \quad (5)$$

where D_m is mass equivalent diameter of bare BC or FeO_x; D_L and D_U are the lower and upper limits, respectively, of the diameter for the integral calculus; $dM_{BC}/d\log D_m$ and $dM_{FeOx}/d\log D_m$ are the mass size distributions of BC and FeO_x, respectively; and MAC_{Mie_BC} (D_m, λ) and MAC_{Mie_FeOx} (D_m, λ) are the MAC values of bare BC and FeO_x, respectively, for D_m and λ calculated by Mie theory.

The mass size distributions of BC and FeO_x at Fukue and Ny-Ålesund (Fig. 2) were obtained by fitting monomodal and bimodal lognormal functions to the average mass size distributions measured by the SP2 during each observation campaign (Yoshida et al., 2020). The measurements at Fukue were made in April 2019 and those at Ny-Ålesund in March 2017. The MAC_{Mie_BC} (D_m, λ) and MAC_{Mie_FeOx} (D_m, λ) data (Fig. 2) were calculated by Mie theory for λ = 565 nm (wavelength used for COSMOS). For this calculation, we assumed BC and FeO_x to be in the form of bare spheres with void-free densities of 1.80 g cm^{-3} and 5.17 g cm^{-3}, respectively. The refractive index of BC we used was 1.99 + 0.64*i*, which is the value for BC at λ = 600 nm (Bergstrom, 1972). The refractive index of FeO_x we used was 2.56 + 0.57*i*, which is the value for magnetite at λ = 600 nm (Huffman and Stapp, 1973).

From Eq. (4), the ε values at Fukue and Ny-Ålesund were calculated to be 3.6 % and 1.9 %, respectively, for (D_L, D_U) = (30, 1000 nm). These ε values became 4.6 % and 2.6 % for (D_L, D_U) = (30, 2500 nm). Because COSMOS is equipped with a PM_1 cyclone, we estimated the effect of light absorption by FeO_x on M_{BC} measured by COSMOS to be < 4 % in East Asia and < 2 % in the Arctic. Note that these estimates are upper limits of the effect of FeO_x because the PM_1 cyclone is designed to remove particles of > 1 μm aerodynamic diameter (D_a). Due to the fractal shape and high density of FeO_x particles (Moteki et al., 2017), D_m is considerably smaller than D_a for FeO_x particles and thus D_U in Eq. (4) should be less than 1 μm.

The effect of FeO_x on M_{BC} (COSMOS) should be even smaller considering that the mass concentration of anthropogenic FeO_x is correlated with M_{BC}, as mentioned above. Even if b_{abs} (COSMOS) is enhanced by FeO_x by a few percent, this effect is already incorporated to some extent, by operationally defining MAC (COSMOS, SP2) by Eq. (2).

The effect of FeO_x on b_{abs} may be somewhat higher for the other filter-based absorption photometers than for COSMOS if they are equipped with a larger particle size cut ($PM_{2.5}$ or PM_{10}). For accurate measurements of M_{BC}, the use of a PM_1 cyclone or impactor is recommended to minimize the effects of FeO_x, as well as other refractory particles such as natural dust and sea-salt particles.

2.2.3 Filter-based absorption photometers other than COSMOS

2.2.3.1 PSAP and CLAP

The principle of operation of the PSAP is similar to those of COSMOS (Bond et al., 1999; Sinha et al., 2017). In this study, we also used b_{abs} data obtained with a continuous light absorption photometer (CLAP) (Ogren et al., 2017). The CLAP is conceptually similar to the PSAP but uses solenoid valves to cycle through eight sample filter spots. The PSAP and CLAP both utilize the Pallflex filters. The unit-to-unit variations of the PSAP and CLAP were reported to be within 6 % (Bond et al.,1999) and 4 % (Ogren et al., 2017), respectively. The wavelengths of the light absorption measured by either PSAP or CLAP at Barrow, Ny-Ålesund, and Alert were about 467, 530, and 660 nm. The major difference of the PSAP and CLAP from the COSMOS is that the sample air inlets of the PSAP and CLAP are not heated to 300°C. Therefore, the effect of the attenuation of light by LSPs is corrected for by using the aerosol light scattering coefficient simultaneously measured by an integrating nephelometer (Bond et al., 1999; Ogren, 2010). This correction adjusts for measurement artifacts but introduces uncertainties in the estimate of b_{abs} (PSAP or CLAP). At the above three sites, light scattering coefficients measured by nephelometers at wavelengths of 450, 550, and 700 nm were used for this correction. The b_{abs} for the PSAP or CLAP (hereafter, b_{abs} (PSAP/CLAP)) at λ = 550 nm was obtained by adjusting measured absorption at 530 to 550 nm by using the λ^{-1} relationship (Sinha et al., 2017; Sharma et al., 2017). Schmeisser et al. (2017) reported that the median value of the absorption Ångström exponent at Arctic sites was 1.04, which supports our assumption of the λ^{-1} relationship. The accuracy of the b_{abs} measured by PSAP ranges between 20 and 30 % (Bond et al., 2013). Note that a custom-built PSAP (Krecl et al., 2007) was used at Ny-Ålesund and commercial ones were used at Alert and Barrow.

2.2.3.2 Aethalometer

An AE-31 Aethalometer (Hansen et al., 1984) has been used for measurements of b_{abs} at Alert without any particle size cut (Sharma et al., 2017). This Aethalometer measures the attenuation (ATN) of light transmitted through particles accumulating on a quartz fiber filter at seven wavelengths (370, 470, 520, 590, 660, 880, and 950 nm). In deriving b_{abs} (Aethalometer) from ATN data, the correction factor C_f = 3.45 (Backman et al., 2017) was applied. This correction factor is very close to the correction factor C_0 = 3.5 recommended by the World Meteorological Organization/Global Atmosphere Watch (WMO/GAW, 2016). The uncertainty of C_0 is approximately 25 % (WMO/GAW, 2016).

Another AE-31 Aethalometer has also been used at Ny-Ålesund (Zeppelin station) (Eleftheriadis et al., 2009), where the sampling inlet was equipped with a calculated PM_{10} size cut. Data post-processing included flagging based on Zeppelin station logs, Ny-Ålesund harbor logs and diagnostics reported by the instrument (flowrate, raw attenuation, zero signal, etc). A correction factor C_0 = 3.5 was used to compensate for the multiple scattering effect.

The filter loading effect is not significant for Arctic aerosol, as reported by Backman et al. (2017). For Alert, the slope of the correction factor Cf-1 to ATN is k = 0.00074, indicating a 5 % difference at an ATN value of 80. For Zeppelin, the loading effect causes a 2 % difference in Cf at an attenuation value of 80. These uncertainties are considered small compared to the overall b_{abs} uncertainty, which is 20–30 % (Bond et al., 2013). Therefore, the loading correction is not applied to the AE31 measurements. Corrections for light scattering by using nephelometer data were also not applied. One of the manufacturer's suggested values of MAC (Aethalometer) is given by 14625 / (λ [nm] $\times C_0$) [m^2 g^{-1}] which corresponds to 7.1 m^2 g^{-1} for λ = 590 nm and C_0 = 3.5.

2.2.3.3 MAAP

Detailed descriptions of the MAAP are given elsewhere (Petzold et al., 2002, 2005; Petzold and Schönlinner, 2004; Kanaya et al., 2013). In brief, the MAAP monitors the transmittance of light through a glass-fiber tape and measures reflectance at two angles. To remove the influence of LSPs, b_{abs} (MAAP) from particles deposited on the filter is derived by radiative transfer calculations. The uncertainty of b_{abs} (MAAP) was estimated by Petzold and Schönlinner (2004) to be 12 %. The unit-to-unit variation of the MAAP was reported to be within 5 % (Müller et al., 2011). The MAC values for the MAAP (MAC (MAAP)) for λ = 637 nm was determined by comparing b_{abs} (MAAP) and M_{BC} measured at four sites in Germany by the German reference method VDI2465 Part 1 (GRM; Schmid et al., 2001), represented by

$$\mathrm{MAC\ (MAAP, GRM)} \equiv \frac{b_{abs}\,(\mathrm{MAAP})}{M_{BC}\,(\mathrm{GRM})}. \qquad (5)$$

For the measurements of M_{BC} (GRM), organic carbon was removed by solvent extraction and the residual BC particles on the filters were oxidized to CO_2 and quantified by coulometric titration. The measurement uncertainty of M_{BC} (GRM) was about 25 % (Petzold and Schönlinner, 2004). The MAC of 6.6 m^2 g^{-1} is the default setting by the manufacturer based on their study. In determining MAC (MAAP, GRM), an SP2 was not used to measure M_{BC}, and this is a potential source of discrepancy in this value of MAC, as discussed in Sect. 3.4.1 and 3.5.2. A correction factor of 1.05 due to the wavelength shift from the nominal value (Müller et al., 2011) was applied in this study. Note that the measured peak wavelength of the light source of the MAAP at Fukue was 639 nm (Kanaya et al., 2013), which is very slightly different from the previously reported value (637 nm; Müller et al., 2011).

3 Results and discussion

3.1 Alert

3.1.1 COSMOS-SP2 comparison

Long-term measurements of BC using different model versions of SP2s have been conducted at Alert since 2011 (Sharma et al., 2017). In this study, we used the data obtained by an EC-SP2 (model "SP2-D" with eight channels; see Sect. 2.2.1) from January to May 2018 for comparison with the COSMOS data. The EC-SP2 and COSMOS aspired sample air from a common inlet with a PM_1 size cut. Fig. 3a shows the number and mass size distributions of BC averaged over the observation period. The mode diameter of the average mass size distribution of BC was ~210 nm in mass-equivalent diameter, which is similar to that previously reported at Alert (Sharma et al., 2017) and to that observed by aircraft-based measurements over Alert (Schulz et al., 2019). Because the upper limit of the detectable diameter range of BC was ~600 nm for the EC-SP2, we have estimated M_{BC} (SP2) over the range up to 1000 nm by fitting lognormal functions to the measured mass size distributions. The time series of hourly values of M_{BC} (COSMOS) and M_{BC} (SP2) (Fig. 3b) were strongly correlated (r^2 = 0.92; r^2 is the square of the correlation coefficient) and the slope of the regression forced through the origin was 1.02 (Fig. 3c). Based on the slope value of the regression for whole M_{BC} ranges observed, the agreement between M_{BC} (COSMOS) and M_{BC} (SP2) at Alert was generally within 10 %. The degree of agreement between M_{BC} (COSMOS) and M_{BC} (SP2) was also examined on a logarithmic scale in Fig. S1a in the Supplement. When M_{BC} (SP2) is relatively low (M_{BC} < 10 ng m^{-3}), which corresponds to the monthly-averaged M_{BC} ranges in summer at Arctic sites (Sinha et al., 2017), M_{BC} (COSMOS) tended to be higher than M_{BC} (SP2) by about 1–2 ng m^{-3}. This small absolute difference is consistent with the previously reported difference between M_{BC} (COSMOS) and M_{EC} at Barrow (Sinha et al., 2017).

Although this agreement between M_{BC} (COSMOS) and M_{BC} (SP2) at Alert was consistent with those reported in previous studies using UT-SP2 (Kondo et al., 2011; Ohata et. al., 2019), note that there were some differences between M_{BC} (SP2) measured by the EC-SP2 and that by the UT-SP2. The EC-SP2 was calibrated using Aquadag samples at Alert during the observation period and also calibrated using fullerene soot samples at the Paul Scherrer Institute in Switzerland after the observation period. Because the sensitivity of the incandescence signals of the SP2 to Aquadag is higher than that to fullerene soot, the calibration curve for Aquadag needs correction to obtain the fullerene-soot equivalent calibration curve (Baumgardner et al., 2012). Additionally, to make this correction, assumptions of the effective density (ρ_{eff}) values of Aquadag (Moteki and Kondo, 2010; Gysel et al., 2011), which depend on the mobility diameter of Aquadag, are needed since a differential mobility analyzer (DMA) is used for the on-site calibration at Alert instead of an aerosol particle mass analyzer (APM) or a centrifugal particle mass analyzer. The ρ_{eff} values of Aquadag samples can depend on their batches (Gysel et al., 2011). In the previous study by Sharma et al. (2017), the constant value of ρ_{eff} (= 0.7 g cm^{-3}) for Aquadag was assumed in order to derive M_{BC} (SP2) at Alert. However, we have found that M_{BC} (SP2) at Alert was highly dependent on the assumed ρ_{eff} values of Aquadag used for the on-site calibration with a DMA. Because of this, we used the calibration curve obtained by fullerene soot with an APM at the Paul Scherrer Institute after the observation period for this study. The conditions of the EC-SP2 might have differed slightly during and after the observation period, which may lead to additional uncertainties for

M_{BC} (SP2) at Alert, although the difference between Aquadag calibrations made before and after the campaign was less than about 10 %. In addition, the upper limit of the detectable diameter of BC for the EC-SP2 (D_m ~600 nm) was lower than that for the UT-SP2 (D_m ~850 nm), although the above-mentioned extrapolation up to 1000 nm was made to derive M_{BC} (SP2) at Alert. Despite these differences between EC-SP2 and UT-SP2, M_{BC} (COSMOS) and M_{BC} (SP2) agree to within 10 % at Alert, consistent with previous studies that reported the stability of the relationship between M_{BC} (COSMOS) and M_{BC} (SP2) at various sites (Kondo et al., 2011; Ohata et. al., 2019).

3.1.2 COSMOS-PSAP comparison

Measurements of M_{BC} (COSMOS) at Alert began in January 2018. A PM_1 cyclone was used for the COSMOS and a PM_1 impactor for the PSAP and two CLAP instruments (CLAP1, CLAP2). The time series of 1-h and 24-h averaged M_{BC} (COSMOS) were strongly correlated with b_{abs} (PSAP; λ = 550 nm) for 2018–2019 (r^2 ~0.96; Fig. 4a–d). In this study, we define the MAC value, MAC_{cor}, as the slope of the least squares regression forced through the origin in the correlation plot. The values of MAC_{cor} (PSAP; λ= 550 nm) for the whole period were 13.9 m^2 g^{-1} and 14.0 m^2 g^{-1} for the 1-h and 24-h averaged data, respectively, as summarized in Table 2. The results of the same analyses for other wavelengths of the PSAP and the two CLAPs show that the strength of the correlation depended little on wavelength (Table 2). The b_{abs}, and therefore the MAC, for the PSAP and the two CLAP instruments (CLAP1, CLAP2) agree to within 13 % at λ = 550 nm, indicating a small difference in the performance of these instruments.

Along with the correlation analysis, variability of the b_{abs} (PSAP) / M_{BC} (COSMOS) ratio was also analyzed for the 1-h and 24-h data (Fig. 4e and f). This ratio can be interpreted as an hourly or daily MAC value at each time. Because this ratio tends to be unstable when the M_{BC} (COSMOS) values are very low, we set a threshold M_{BC} (COSMOS) value of 2 ng m^{-3} in this analysis, as shown in these figures. The median ratio, defined as median MAC and denoted as MAC_{med}, was 13.5 m^2 g^{-1} for both 1-h and 24-h data, which is very close to MAC_{cor} (13.9 m^2 g^{-1} and 14.0 m^2 g^{-1} for the 1-h and 24-h data, respectively) (Table 3). The difference between MAC_{cor} and MAC_{med} was about 4 %, leading to the same difference between the estimated M_{BC} values if these MAC values are used for conversion of b_{abs} (PSAP) to M_{BC}. Based on the interquartile ranges of the b_{abs} (PSAP) / M_{BC} (COSMOS) ratios (Fig. 4e and f), variations of the ratios (with an M_{BC} threshold of 2 ng m^{-3}), denoted as V_{MAC}, were within 19 % and 18 % of the MAC_{med} values for the 1-h and 24-h data, respectively (Table 3). Therefore, conversion of 1-h and 24-h averaged b_{abs} (PSAP; λ = 550 nm) data to M_{BC} by assuming a constant MAC_{med} leads to uncertainty of about 19 % at Alert. We used the same method in estimating MAC_{cor}, MAC_{med}, and V_{MAC} for other instruments and other locations, as summarized in Table 3. Note that this estimated uncertainty can depend on the threshold value of M_{BC} (COSMOS) assumed in the analysis. Fig. S2 in the Supplement shows histograms of the b_{abs} (PSAP) / M_{BC} (COSMOS) ratios for M_{BC} (COSMOS) < 10 ng m^{-3}. While similar MAC_{med} values were obtained for data with M_{BC} (COSMOS) < 10 ng m^{-3} and for all dataset, the interquartile ranges of the b_{abs} (PSAP) / M_{BC} (COSMOS) ratios are larger for M_{BC} (COSMOS) < 10 ng m^{-3}. The relative uncertainty becomes higher (lower) in summer (winter/spring) when the M_{BC} values tend to be low (high) (Fig. 4a and b).

3.1.3 COSMOS–Aethalometer comparison

Measurements of b_{abs} at Alert were made by an Aethalometer at wavelengths of 370, 470, 520, 590, 660, 880, and 950 nm without any particle size cut. Time series of b_{abs} (Aethalometer; λ = 590 nm) and M_{BC} (COSMOS) in 2018–2019 are shown in Fig. S3a and b in the Supplement. b_{abs} (Aethalometer; λ = 590 nm) was highly correlated ($r^2 > 0.90$) with M_{BC} (COSMOS) (Fig 5a and b). The MAC_{cor} (Aethalometer; λ = 590 nm) values were 12.5 and 12.7 m^2 g^{-1} for the 1-h and 24-h data, respectively. The MAC_{med} values of the b_{abs} (Aethalometer) / M_{BC} (COSMOS) ratios were 13.5 m^2 g^{-1} and 13.8 m^2 g^{-1} for the 1-h and 24-h data, respectively (Fig. 5c and d), which agree with the MAC_{cor} values to within 8 %. Therefore, depending on the MAC values used, the estimated M_{BC} values can differ by about 8 %. Because the interquartile ranges of the b_{abs} (Aethalometer) / M_{BC} (COSMOS) ratios were 11.4–16.5 m^2 g^{-1} (1-h data) and 12.1–15.7 m^2 g^{-1} (24-h data), the V_{MAC} was about 22 % (with an M_{BC} threshold of 2 ng m^{-3}) for b_{abs} (Aethalometer; λ = 590 nm) at Alert (Table 3). The MAC_{med} values for low M_{BC} data (M_{BC} (COSMOS) < 10 ng m^{-3}) agree with those for all datasets to within 10 % (Fig S3c and d in the Supplement).

The MAC_{cor} (Aethalometer) values for each wavelength are summarized in Table 4. Note that these wavelength-dependent MAC_{cor} values should be interpreted as the simple conversion factors to obtain average M_{BC} from b_{abs} (Aethalometer), which might have been contributed to by BC and also other light-absorbing aerosols. In other words, these MAC_{cor} values differ from MAC_{BC}, as discussed in Sect. 1. The r^2 values were generally high for all wavelengths examined. This weak dependence on wavelength indicates that the contribution of other light-absorbing aerosols such as brown carbon (BrC) to b_{abs} (Aethalometer) is small or the BrC/BC concentration ratio was rather stable at Alert during 2018–2019, because BrC should enhance light absorption in near ultraviolet wavelengths.

The MAC_{cor} (Aethalometer) and MAC_{cor} (PSAP) are compared in Table 5. They agree within 10 % at three wavelengths, despite the different particle size cuts of the inlets for Aethalometer (total suspended particle) and PSAP (PM_1). This agreement is consistent with the results by Backman et al. (2017), who showed that the correction factor C_f of 3.45 for Aethalometer harmonizes b_{abs} (Aethalometer) with b_{abs} (PSAP), b_{abs} (CLAP), and b_{abs} (MAAP) at Arctic sites.

3.2 Ny-Ålesund

3.2.1 COSMOS-PSAP comparison

Simultaneous measurements of M_{BC} (COSMOS) for PM_1 and b_{abs} (PSAP) for PM_{10} began at Ny-Ålesund in 2012 (Sinha et al., 2017; Fig. S4a and b in the Supplement). The 1-h and 24-h averaged b_{abs} (PSAP; λ = 550 nm) were well correlated (r^2 = 0.76–0.82) with M_{BC} (COSMOS), and the MAC_{cor} (PSAP) value for the whole period was 14.4–15.2 m^2 g^{-1} (Fig. 6a and b). Year-to-year variations of MAC_{cor} (PSAP) are also shown in Fig. 7a and Table 6. The correlation between b_{abs} (PSAP) and M_{BC} (COSMOS) during April–December 2012 was weak for unknown reasons. Excluding this period, average MAC_{cor} (PSAP) during 2013–2016 was 15.2 ± 2.2 (1σ) and 16.6 ± 1.4 m^2 g^{-1} for the 1-h and 24-h data, respectively. Although the reason for the relatively large change in MAC_{cor} (PSAP) values during 2014–2015 (Fig. 7a and Table 6) is not clear, this may be partly because b_{abs} (PSAP) data from December 2014 to April 2015 (during an "Arctic haze" period) were not available (Fig. S4a and b in the Supplement).

The MAC_{med} values of the b_{abs} (PSAP) / M_{BC} (COSMOS) ratios were 16.7 and 17.2 m^2 g^{-1} for the 1-h and 24-h data, respectively, when the M_{BC} threshold of 2 ng m^{-3} was applied in the analysis (Fig. 6c and d). The MAC_{med} values were by 16 % and 13 % higher than MAC_{cor} for 1-h and 24-h data, respectively (Table 3). Therefore, conversion of b_{abs} (PSAP; λ = 550 nm) to M_{BC} using a constant MAC_{cor} may result in a slightly biased M_{BC}, especially for lower b_{abs} data. This is partly because the correlation of b_{abs} (PSAP) with M_{BC} (COSMOS) is not very high and scatter of the data, especially those with lower M_{BC} values, contributes to large variations of the b_{abs} (PSAP) / M_{BC} (COSMOS) ratios (Fig. 6 and Fig. S4c and d in the Supplement). The interquartile range of the ratios were 10.6–21.7 m^2 g^{-1} and 11.9–21.4 m^2 g^{-1} for the 1-h and 24-h data, respectively. Although these large variations might be partly attributed to actual variations in mixing states of BC, artifacts of b_{abs} measurements by PSAP at Ny-Ålesund may be a contributing factor, considering the higher correlations of b_{abs} (Aethalometer) and b_{abs} (MAAP) at Ny-Ålesund with M_{BC} (COSMOS) (Sect. 3.2.2 and 3.2.3). Based on the interquartile ranges of the b_{abs} (PSAP) / M_{BC} (COSMOS) ratios, V_{MAC} was 37% and 31% for 1-h and 24-h data, respectively (Table 3). The above-mentioned bias leads to an additional uncertainty of about 15 % for the estimates of M_{BC}, if the constant MAC_{cor} value is used.

3.2.2 COSMOS-Aethalometer comparison

Measurements of b_{abs} (Aethalometer; λ = 590 nm) for PM_{10} were compared with measurements of M_{BC} (COSMOS) for PM_1 during 2012–2019. The time series data of b_{abs} (Aethalometer) were highly correlated with those for M_{BC} (COSMOS) (Fig. S5a and b in the Supplement) (r^2 = 0.90 for both the 1-h and 24-h data; Fig. 8a and b). The MAC_{cor} (Aethalometer) values were 10.2 and 10.1 m^2 g^{-1} for the 1-h and 24-h data, respectively. Year-to-year variations of MAC_{cor} (Aethalometer) are also shown in Fig. 7a and Table 7. The r^2 values were generally high for each year and the average MAC_{cor} (Aethalometer) during 2012–2019 was 10.2 ± 1.6 (1σ) and 10.0 ± 1.3 m^2 g^{-1} for the 1-h and 24-h data, respectively. The MAC_{cor} (Aethalometer) value for 2012 was 8.7 m^2 g^{-1} at 590 nm (i.e., 9.3 m^2 g^{-1} at 550 nm assuming the λ^{-1} relationship) for 24-h data, which is consistent with the MAC_{cor} of 9.8 m^2 g^{-1} at 550 nm inferred from the SP2 and Aethalometer measurements in the spring of 2012 (Zanatta et al., 2018). At Ny-Ålesund, the MAC_{cor} (Aethalometer) values (10.2 and 10.1 m^2 g^{-1} for the 1-h and 24-h data, respectively) were systematically lower than the MAC_{cor} (PSAP) values (14.4 m^2 g^{-1} and 15.2 m^2 g^{-1}). This discrepancy is different than at Alert (Sect. 3.1.3) and the reason is unclear, but could be partly due to uncertainty in the absolute values of b_{abs}, as discussed in Sect. 1 and Sect. 2.2.3.

The MAC_{med} values of the b_{abs} (Aethalometer) / M_{BC} (COSMOS) ratios were 11.2 and 12.3 m^2 g^{-1} for the 1-h and 24-h data, respectively (Fig. 8c and d). While the MAC_{med} for the 1-h data agree with MAC_{cor} to within 10 %, there is a 22 % discrepancy for the 24-h data under the assumed threshold setting (2 ng m^{-3}) of M_{BC} (COSMOS) (Table 3). Therefore, conversion of 24-h averaged b_{abs} (Aethalometer; λ = 590 nm) to M_{BC} using a constant MAC_{cor} may be somewhat biased, especially for lower b_{abs} values (Fig S5c and d in the Supplement). At Ny-Ålesund, the V_{MAC} was about 25 % for b_{abs} (Aethalometer; λ = 590 nm). The above-mentioned bias leads to an additional uncertainty of about 20 % for conversion of 24-averaged low b_{abs} data to M_{BC}, if the constant MAC_{cor} value is assumed.

3.2.3 COSMOS-MAAP comparison

Measurements of b_{abs} (MAAP; λ = 637 nm) without any particle size cut were compared with measurements of M_{BC} (COSMOS) for PM_1 during 2017–2020. The time series of b_{abs} (MAAP) and M_{BC} (COSMOS) tracked each other (Fig. S6a and b in the Supplement) and were highly correlated (r^2 = 0.90 for the 1-h data and r^2 = 0.83 for the 24-h data; Fig. 9a and b). The MAC_{cor} (MAAP) values were 10.6 and 10.9 m^2 g^{-1} for the 1-h and 24-h data, respectively. These MAC_{cor} values are about 60 % higher than the manufacturer's default setting (= 6.6 m^2 g^{-1}) of MAC (MAAP). One possible reason is the difference of the methods of M_{BC} measurements to determine MAC_{cor} (MAAP) values, as mentioned in Sect. 2.2.3.3. Another reason could be that the difference in microphysical properties of BC (mixing states and size distribution) and properties of LSPs led to the difference in the MAC_{cor} (MAAP) values.

Year-to-year variations of MAC_{cor} (MAAP) are also shown in Fig. 7a and Table 8. The r^2 values were generally high for each year and the average MAC_{cor} (MAAP) during 2017–2020 was 11.1 ± 0.7 (1σ) and 11.7 ± 1.1 m^2 g^{-1} for the 1-h and 24-h data, respectively. The MAC_{med} values of the b_{abs} (MAAP) / M_{BC} (COSMOS) ratios were 10.8 and 11.2 m^2 g^{-1} for the 1-h and 24-h data, respectively (Fig. 9c and d). The difference between MAC_{cor} and MAC_{med} was limited to 3 % (Table 3). As discussed for the PSAP and Aethalometer in the previous sections, the relative uncertainty becomes higher when the M_{BC} values tend to be low (Fig. S6c and d in the Supplement).

The MAC_{cor} (MAAP) and MAC_{cor} (PSAP) at Ny-Ålesund are compared in Table 11 in Sect. 3.6 after adjusting measurement wavelengths. MAC_{cor} (PSAP) values are 17 % and 20 % larger than MAC_{cor} (MAAP) values for 1-h and 24-h data, respectively. A custom-built PSAP was used at Ny-Ålesund. The systematic difference of b_{abs} measured by the custom-built PSAP and MAAP was also observed at 3 European background sites (Zanatta et al., 2016), although the previously reported difference was much larger (more than 59 %) than that of our measurements at Ny-Ålesund.

3.3 Barrow

3.3.1 COSMOS-PSAP/CLAP comparison

Simultaneous measurements of PM_1 for M_{BC} (COSMOS) and b_{abs} (PSAP/CLAP) began at Barrow in 2012 (Sinha et al., 2017). At Barrow, both the PSAP and CLAP aspired ambient air using PM_1 and PM_{10} impactors alternately for 30 min of each hour. Here we used the data from the PSAP/CLAP equipped with the PM_1 impactor and data from the PSAP in 2012–2015 and the CLAP in 2016–2019 (Fig. S7 in the Supplement). Because the 24-h averaged b_{abs} (PSAP) and b_{abs} (CLAP) values agreed to within 2 % during 2012–2015 (Sinha et al., 2017) when the PSAP and CLAP overlapped, we consider the two instruments to be equivalent. The M_{BC} (COSMOS) data from June 2018 to May 2019 were unavailable due to problems with the COSMOS instrument.

The b_{abs} (PSAP/CLAP; λ = 550 nm) data were strongly correlated with those for M_{BC} (COSMOS) (r^2 = 0.88 and r^2 = 0.86; Fig. 10a and b) and the MAC_{cor} (PSAP/CLAP) derived from 1-h and 24-h averaged data for the whole period were 10.8 and 10.6 $m^2\ g^{-1}$, respectively. Average MAC_{cor} (PSAP/CLAP) during 2012–2018 was stable at 11.0 ± 0.9 (1σ) $m^2\ g^{-1}$ (Fig. 7b and Table 9). Yearly M_{BC} (COSMOS) values did not exhibit large changes during this period (Fig. 7b). The b_{abs} (CLAP) data was weakly correlated with M_{BC} (COSMOS) data during June–December 2019 (Table 9), indicating that either the CLAP or COSMOS results might not have been accurate during this period. Therefore, in Table 9 we calculated the average MAC_{cor} (PSAP/CLAP) by excluding the MAC value for 2019.

The MAC_{med} values of the b_{abs} (PSAP/CLAP) / M_{BC} (COSMOS) ratios were 11.2 and 11.0 $m^2\ g^{-1}$ for 1-h and 24-h data (Fig. 10c and d), which are very close to the MAC_{cor} values of 10.8 and 10.6 $m^2\ g^{-1}$, respectively (Table 3). Therefore, when either MAC_{cor} or MAC_{med} is used for conversion of b_{abs} (PSAP/CLAP; λ = 550 nm) to M_{BC}, the resulting M_{BC} values differ by only about 4 %. The V_{MAC} was about 25 % for b_{abs} (PSAP /CLAP; λ = 550 nm) at Barrow (Table 3). Because of scatter in the data, especially at lower M_{BC} values (Fig. 10a and b), the interquartile ranges of the b_{abs} (PSAP) / M_{BC} (COSMOS) ratios are much larger when M_{BC} (COSMOS) is less than 10 ng m^{-3} (Fig. S7c and d).

3.4 Pallas

3.4.1 COSMOS-MAAP comparison

Measurements of b_{abs} (MAAP; λ = 637 nm) have been made since 2007 at the Global Atmospheric Watch (GAW) station at Pallas (Hyvärinen et al., 2011). PM_{10} and PM_1 inlets were used for MAAP and COSMOS, respectively. M_{BC} (COSMOS) measurements began in July 2019; we used the data collected up to July 2020 in this study. The M_{BC} (COSMOS) data for about 3 months (February to April 2020) were unavailable due to an air sampling problem.

The b_{abs} (MAAP) 1-h and 24-h values (Fig. S8 in the Supplement) were strongly correlated with those for M_{BC} (COSMOS) with r^2 = 0.93 and r^2 = 0.95, respectively (Fig. 11a and b). MAC_{cor} (MAAP) was 13.0 m^2 g^{-1} for both the 1-h and 24-h data. This MAC_{cor} value is about twice the manufacturer's default setting (= 6.6 m^2 g^{-1}) of MAC (MAAP), possibly for the same reasons discussed in Sect. 3.2.3.

The MAC_{med} values of the b_{abs} (MAAP) / M_{BC} (COSMOS) ratios for the 1-h and 24-h data were 12.4 and 13.1 m^2 g^{-1}, respectively (Fig. 11c and d), which are very close to that for MAC_{cor} (13.0 m^2 g^{-1} for both 1-h and 24-h data, Table 3). Therefore, the difference between the estimated M_{BC} values is less than 5 % when these MAC_{cor} or MAC_{med} values are used for conversion of b_{abs} (MAAP) to M_{BC}. The V_{MAC} was about 25 % for b_{abs} (MAAP) at Pallas (Table 3). The MAC_{med} values for low M_{BC} data (M_{BC} (COSMOS) < 10 ng m^{-3}) are very close to those for all dataset (Fig S8c and d in the Supplement).

3.5 Fukue Island

3.5.1 COSMOS-SP2 comparison

The UT-SP2 was operated at Fukue for 3 weeks in April 2019 (Yoshida et al., 2020), as mentioned in Sect. 2.2.1. Fig. 12a shows the number and mass size distributions of BC measured by the UT-SP2 averaged over the observation period. In addition to the M_{BC} (SP2) derived by integrating the mass size distributions over the detectable diameter range (D_m = 70–850 nm), we also estimated M_{BC} (SP2) in the D_m = 30–1000 nm range by fitting a lognormal function to the data. As the two sets of M_{BC} (SP2) values deviated by less than 2 %, we used the former M_{BC} (SP2) for comparison with M_{BC} (COSMOS). The time series of hourly values of M_{BC} (COSMOS) were strongly correlated (r^2 = 0.97) with M_{BC} (SP2) (Fig. 12b) and the slope of the regression was 0.92 (Fig. 12c). This relationship agrees with those observed by Ohata et al. (2019) at Tokyo, Cape Hedo, and Ny-Ålesund and those observed at Alert (Sect. 3.1.1), thus confirming the clear and consistent relationship between M_{BC} (COSMOS) and M_{BC} (SP2). Miyakawa et al. (2017) also reported a strong correlation (r^2 = 0.92; regression slope 1.14) between M_{BC} (COSMOS) and M_{BC} (SP2) at Fukue in spring 2015 by using an SP2 maintained and calibrated by the Japan Agency for Marine-Earth Science and Technology.

The degree of agreement between M_{BC} (COSMOS) and M_{BC} (SP2) at Fukue was also examined on a logarithmic scale in Fig. S1b in the Supplement. When M_{BC} (SP2) is lower than ~70 ng m^{-3}, M_{BC} (COSMOS) tended to be slightly higher than M_{BC} (SP2). A similar feature was previously reported at Cape Hedo in Japan (Ohata et al., 2019). The Cape Hedo site is located near the coast (i.e., the distance of this site to the coast is ~0.2 km) and the interference of submicron sea salt particles might contribute to this feature (Ohata et al., 2019). At Fukue, when maritime air mass is transported to the site, the relative abundance of sea salt particles to BC might be also enhanced possibly affecting the COSMOS measurements, although the distance from the site to the coast (~1.5 km) is slightly farther than for Cape Hedo. This feature was not clearly observed by a previous study at Fukue (Miyakawa et al., 2017).

3.5.2 COSMOS-MAAP comparison

Kanaya et al. (2013, 2016, 2020) made simultaneous measurements of M_{BC} (COSMOS) and b_{abs} (MAAP; λ = 639 nm) at Fukue for about 10 years (April 2009–May 2019; Fig. S9 in the Supplement). The air inlet for the MAAP and COSMOS was equipped with a PM_1 cyclone after November 2011. Before that a PM2.5 cyclone was used instead. b_{abs} (MAAP) was highly correlated (r^2 = 0.94) with M_{BC} (COSMOS) and the MAC_{cor} (MAAP) for the entire period was found to be 10.8 m^2 g^{-1} and 10.9 m^2 g^{-1} for the 1-h and 24-h data (Fig. 13a and b), respectively. Because the correlation of b_{abs} (MAAP) with M_{BC} (COSMOS) was also strong for individual years, MAC_{cor} (MAAP) for each year was also derived (Fig. 7c and Table 10). M_{BC} (COSMOS) decreased by about 50 % during this period, owing to a large decrease of BC emissions in China (Kanaya et al., 2020). However, the yearly average MAC_{cor} (MAAP) values were stable at 11.1 ± 1.0 (1σ) m^2 g^{-1} for both the 1-h and 24-h data, despite the large change in M_{BC} (COSMOS). This MAC_{cor} value is about 70 % higher than the manufacturer's default setting (= 6.6 m^2 g^{-1}), possibly for the same reasons discussed in Sect. 3.2.3.

Because the amount of data with M_{BC} less than 2 ng m^{-3} was very small at Fukue, the MAC_{med} values and the interquartile ranges of the b_{abs} (MAAP) / M_{BC} (COSMOS) ratios were obtained for all data without applying any M_{BC} threshold. The MAC_{med} was 11.4 m^2 g^{-1} for both 1-h and 24-h data (Fig. 13c and d), which agrees well (within 6 %) with the MAC_{cor} values derived from correlation plots (10.8 and 10.9 m^2 g^{-1} for 1-h and 24-h data, respectively) (Table 3). Therefore, using either MAC_{cor} or MAC_{med} for conversion of b_{abs} (MAAP) to M_{BC} affects the resulting M_{BC} values by less than 6 %. The V_{MAC} was about 15 %, which is lower than those at Arctic sites (Table 3) partly because the higher M_{BC} (COSMOS) values at Fukue make the calculated ratios more stable. Also, aerosol properties including mixing states of BC might be more stable at Fukue than those at the Arctic sites examined in this study.

3.6 Spatial variability of MAC_{cor} and r^2

In previous sections, we showed that the MAC_{cor} values depended on instrument and observation site. The values of MAC_{cor} (λ = 550 nm) and r^2 are summarized in Table 11. Here, the MAC_{cor} (MAAP; λ

~637 nm) and MAC_{cor} (Aethalometer; λ = 590 nm) values were adjusted to those at λ = 550 nm by assuming an absorption Ångstrom exponent of 1.0 (i.e., a λ^{-1} relationship). The unit-to-unit variations of b_{abs} measurements were reported to be within 5 % for MAAP (Müller et al., 2011), 6 % for PSAP (Bond et al.,1999), and 4 % for CLAP (Ogren et al., 2017), if the careful calibration of flows and filter sampling spot sizes of these instruments are made for individual units. Therefore, the spatial variations of MAC_{cor} values observed in this study likely reflects differences of aerosol properties at the observation sites.

The values of MAC_{cor} (PSAP) at Alert and MAC_{cor} (PSAP/CLAP) at Barrow were both determined with a PM_1 size cut and they differed by about 22 % for 1-h data. Differences in aerosol properties including mixing states of BC at these sites could contribute to the different MAC values, although this effect cannot be assessed quantitatively with only this dataset. The correlations of b_{abs} (PSAP) with M_{BC} (COSMOS) at Alert were somewhat higher (r^2 = 0.95–0.96) than those of b_{abs} (PSAP/CLAP) at Barrow (r^2 = 0.86–0.88). The stronger correlation of b_{abs} (PSAP) with M_{BC} (COSMOS) at Alert suggests that environmental conditions including LSP/BC ratios and mixing states of BC were more stable at Alert. We found that, at Alert, b_{abs} (PSAP) data with loading and scattering corrections were strongly correlated with the uncorrected b_{abs} (PSAP) data and the contribution of the loading and scattering corrections was about 35 %, on average. In contrast, at Barrow, the contribution of these corrections was about 63 %. This suggests that at Alert, the LSP/BC ratio was small and stable, and the influence of LSPs on derived b_{abs} (PSAP) was small. The greater distance from continental sources of aerosols at Alert than at Barrow (Fig. 1), may contribute to these observed differences.

At Ny-Ålesund, where a PM_{10} inlet was used, the MAC_{cor} (PSAP) values were higher than those at Alert and Barrow. Also, the r^2 values at Ny-Ålesund (r^2 = 0.76–0.82) were lower than those at Alert. Effects of particles larger than 1 µm including dust and sea salt may partly contribute to the larger MAC and lower r^2 values at Ny-Ålesund.

The MAC_{cor} (PSAP) and MAC_{cor} (Aethalometer) agree to within 4 % for 1-h data at Alert, in spite of the different particle size cut of the inlets. However, they differed by about 24 % for 1-h data at Ny-Ålesund. Although the agreements were somewhat better for 2015–2016 at Ny-Ålesund (Fig. 7a), the reason for the overall discrepancy is unknown. Furthermore, while the MAC_{cor} (PSAP) at Ny-Ålesund was higher than that at Alert, the opposite result was obtained by Aethalometers, which is not easily interpreted.

The values of MAC_{cor} (MAAP) determined at Ny-Ålesund and Pallas differ by about 18 %. This difference may be attributed to the difference of average mixing states of BC and properties of other co-existing aerosols, which were affected by environmental conditions. Because these are the only available MAC_{cor} (MAAP) data sets derived from M_{BC} (COSMOS) in the Arctic, it is difficult to further evaluate spatial variability.

We have shown that in general, b_{abs} values obtained by PSAP, CLAP, Aethalometer, and MAAP were strongly correlated with M_{BC} (COSMOS) at all four Arctic sites, although the strength of the correlations differed somewhat among the sites. Based on the analysis of b_{abs}/M_{BC} variations among these sites, the MAC_{cor} and MAC_{med} were most stable for the PSAP with a PM_1 inlet at Alert and most variable for PSAP with a PM_{10} inlet at Ny-Ålesund (Table 3). The average MAC_{cor} (λ = 550 nm) values at these four Arctic sites were 13.0 ± 1.6 (1σ; 12 % of the average) and 13.1 ± 1.7 (1σ; 13 %) m^2 g^{-1} for 1-h and 24-h data, respectively (Table 11). However, these correlations and resulting MAC_{cor} values may not hold outside the Arctic, where environmental conditions can be very different, especially the mixing states of BC and amount of interference by LSPs.

Zanatta et al. (2016), using M_{EC} measured by the thermal-optical transmittance method with the EUSAAR-2 protocol instead of M_{BC} (COSMOS), reported the average MAC_{cor} value at λ = 637 nm for nine European background sites to be 10.0 m^2 g^{-1}. From this MAC_{cor} (λ = 637 nm) value, the value of MAC_{cor} at λ = 550 nm is calculated to be 11.6 m^2 g^{-1} by assuming an absorption Ångstrom exponent of 1.0. Although their MAC_{cor} values were generally obtained using PM_{10} inlets or without particle size-cuts, their average MAC_{cor} value (= 11.6 m^2 g^{-1}) is about 11 % lower than our average MAC_{cor} value (13.0–13.1 m^2 g^{-1}) at 4 Arctic sites determined in this study. This discrepancy may be partly due to the different methods used to determine absolute mass concentrations of BC.

Mason et al. (2018) derived the values of MAC_{cor} (PSAP) and MAC_{cor} (CLAP) for PM_1 size range in biomass burning and agriculture fire plumes during the SEAC^{4}RS aircraft observation campaign by using M_{BC} (SP2) data. They reported the MAC_{cor} (PSAP; λ = 532 nm) and MAC_{cor} (CLAP; λ = 532 nm) values to be 21.0 and 26.5 m^2 g^{-1}, respectively, which are about 60 % larger than the average MAC_{cor} value (13.0–13.1 m^2 g^{-1}) determined in this study. Although the causes for their very high MAC_{cor} values are not clear, one possible explanation given by Mason et al. (2018) is the considerable amount of additional absorbers other than BC, including tar balls, that might have existed in their samples. Also, strong lensing effects by BC coatings could contribute to the high MAC_{cor} values. Thus, the MAC_{cor} values can be highly dependent on environmental conditions and those reported in the present study are considered to be site-specific values, although the variability (1σ) of our MAC_{cor} values in the 4 Arctic sites was within 13 % of the average MAC_{cor} value for these 4 sites.

4 Summary and conclusions

Long-term measurements of M_{BC} by ground-based instruments are needed to investigate changes in the emission, transport, and deposition of BC. Various types of filter-based absorption photometers, including the particle absorption soot photometer (PSAP), the continuous light absorption photometer (CLAP), the Aethalometer, and the multi-angle absorption photometer (MAAP) have been used in the Arctic. To date, the accuracy of M_{BC} estimated from absorption coefficients (b_{abs}) measured by these instruments have not been adequately assessed, mainly because of a lack of simultaneous and reliable M_{BC} measurements.

In this paper, we introduced a systematic methodology to derive M_{BC} from b_{abs} measured by these instruments. To obtain accurate values of M_{BC}, we used a filter-based absorption photometer with a heated inlet (COSMOS), which we calibrated to within 10 % uncertainty with an SP2 deployed in Tokyo. Individual COSMOS instruments used for field observations were calibrated against the standard COSMOS to within about 10 %. The accuracy of M_{BC} (COSMOS) has previously been demonstrated to be about 15 % by comparison with M_{BC} (SP2) for sites in Asia and the Arctic. The effect on M_{BC} (COSMOS) of interference by light-absorbing FeO_x particles was estimated to be only a few percent, owing partly to the particle-size cut off of 1 μm by the PM_1 cyclone used. This effect may be somewhat higher for the other filter-based absorption photometers equipped with larger particle-size cuts. The two necessary conditions for application of our method are a high correlation of b_{abs} with independently measured M_{BC} and long-term stability of the slope of the regression, which represents MAC_{cor}.

We compared b_{abs} (PSAP/CLAP) with M_{BC} (COSMOS) at Alert (PM_1) for 2 years, Ny-Ålesund (PM_{10}) for 4 years, and Barrow (PM_1) for 7 years. The b_{abs} (PSAP/CLAP) was highly correlated with M_{BC} (COSMOS) at these sites. For 1-h data, the MAC_{cor} (PSAP/CLAP) at λ = 550 nm was 13.9 m^2 g^{-1} at Alert, 14.4 m^2 g^{-1} at Ny-Ålesund, and 10.8 m^2 g^{-1} at Barrow. The V_{MAC} was 19 % at Alert, 37 % at Ny-Ålesund, and 22 % at Barrow (Table 3).

We also compared b_{abs} (Aethalometer) with M_{BC} (COSMOS) at Alert (total suspended particles) for 2 years and at Ny-Ålesund (PM_{10}) for 8 years. They were highly correlated and the MAC_{cor} (Aethalometer; λ = 590 nm) for 1-h data was 12.5 m^2 g^{-1} at Alert and 10.2 m^2 g^{-1} at Ny-Ålesund. One of the manufacturer's suggested MAC (Aethalometer) values is given by 14625 / (λ × C_0) which corresponds to 7.1 m^2 g^{-1} for λ = 590 nm and C_0 = 3.5, and which is considerably lower than the values obtained in our study. The V_{MAC} was 22 % at Alert and 25 % at Ny-Ålesund (Table 3).

The b_{abs} (MAAP) and M_{BC} (COSMOS) were also compared at Ny-Ålesund (total suspended particles) for 4 years, at Pallas (PM_{10}) for about 1 year, and at Fukue (PM_1) for about 10 years. b_{abs} (MAAP) was highly correlated with M_{BC} (COSMOS) at these sites. For 1-h data, The MAC_{cor} (MAAP) at λ = 637 nm was 10.6 m^2 g^{-1} at Ny-Ålesund and 13.0 m^2 g^{-1} at Pallas. The MAC_{med} (MAAP) at λ = 639 nm at Fukue was stable at 11.1 ± 1.0 m^2 g^{-1}, despite a 50 % decrease in M_{BC} (COSMOS) during this period (Fig. 7c). The default setting of MAC (MAAP) by the manufacturer (6.6 m^2 g^{-1}) is about half the MAC_{cor} obtained in this study indicating a similar overestimation of M_{BC} if the default value is used to convert b_{abs} (MAAP) to M_{BC} at these sites. For 1-h data, the V_{MAC} was 20 % at Ny-Ålesund, 27 % at Pallas, and 15 % at Fukue.

Our results show that Arctic M_{BC} can be derived from b_{abs} obtained from PSAP, CLAP, Aethalometer, and MAAP measurements with reasonable accuracy by using the MAC_{cor} obtained from the regression slope of the b_{abs}–M_{BC} correlation, especially for long data-averaging times. However, scatter in b_{abs}–M_{BC} (COSMOS) correlations indicate that the accuracy of this method will be somewhat lower than that achieved by direct measurement of M_{BC} (COSMOS). We also caution that the reliability of the use of b_{abs} data to derive M_{BC} at other locations, especially those outside the Arctic, is unknown. Rigorous comparisons with COSMOS or SP2 data, such as those of this study, are required if use of our method is to expand beyond the Arctic region. Moreover, long-term comparisons are desirable for accurate determination of the MAC_{cor}. Short-term comparisons will be of limited value for understanding the variability of MAC for each instrument and location.

Data availability

The M_{BC} and b_{abs} data set used in this publication is available online (https://ads.nipr.ac.jp/dataset/A20201120-001).

Author contributions

SO, TM, and YKo designed the study, conducted the analyses, and wrote the paper. SS and DV contributed to the field observations and data analysis of SP2, PSAP, CLAP, and Aethalometer at Alert. AH, EAs, JB, and HS contributed to the field observations and data analysis of MAAP at Pallas. EAn contributed to the field observations and data analysis of PSAP and CLAP at Barrow. PT obtained and analyzed PSAP data at Ny-Ålesund. KE and SV obtained and analyzed Aethalometer data at Ny-Ålesund. RK and PZ obtained and analyzed MAAP data at Ny-Ålesund. YKa contributed to the field observations and data analysis of MAAP and COSMOS at Fukue. AY and NM obtained and analyzed SP2 data at Fukue. SO, TM, YKo, MK, YZ, YT, JM, and NO contributed to instrument maintenance and data analysis of COSMOS.

Competing interests

The authors declare that they have no conflicts of interest.

Acknowledgements

We thank Kevin Rawlings and Melody Fraser of Environment and Climate Change (Canada) and CFS Alert for operations and maintenance of the Alert site. We thank Bryan Thomas, Peter Detwiler, and Ross Peterson for supporting the measurements at Barrow. We thank the staff of the Norwegian Polar Institute for supporting the measurements at Ny-Ålesund (Zeppelin). This research was performed by the Environment Research and Technology Development Fund (JPMEERF20142003, JPMEERF20152005, JPMEERF20172003, JPMEERF20182003, JPMEERF20202003, and JPMEERF20205001) of the Environmental Restoration and Conservation Agency of Japan; the Japanese Ministry of Education, Culture, Sports, Science, and Technology; the Japan Society for the Promotion of Science KAKENHI Grants (JP12J06736, JP1604452, JP18H04143, JP19H05699, JP23221001, JP25220101, JP26241003, JP26701004, JP16H01770, JP17H04709, JP18H03363, JP19K20437, JP19K20441, and JP20H00638); the Arctic Challenge for Sustainability (ArCS) project (JPMXD1300000000); the Arctic Challenge for Sustainability II (ArCS II) project (JPMXD1420318865); and a grant for the Global Environmental Research Coordination System from the Ministry of the Environment, Japan (MLIT1753). Pallas and Zeppelin measurements and/or analysis were conducted under the financial support of the ACTRIS by the European Union's Horizon 2020 research and innovation programme under grant agreement no. 654109, partly under the European Union's Horizon 2020 research and innovation program under grant agreement no. 689443 via project iCUPE (Integrative and Comprehensive Understanding on Polar Environments) and the 16ENV02 Black Carbon project of the European Union through the European Metrology Programme for Innovation and Research (EMPIR). The research was also supported by Academy of Finland via project NABCEA (grant no. 29664) and Academy of Finland Flagship funding (grant no. 337552). MAAP measurements at Zeppelin were funded and supported by Swedish Environmental Protection Agency (Naturvårdsverket). E. Andrews contribution to this effort was supported in part by the Atmospheric Radiation Measurement (ARM) user facility, a US Department of Energy (DOE) Office of Science user facility managed by the Biological and Environmental Research program.

References

Arctic Monitoring and Assessment Programme (AMAP): AMAP Assessment 2015: Black carbon and ozone as Arctic climate forcers, Oslo, Norway, pp. vii + 116, 2015.

Asmi, E., Backman, J., Servomaa, H., Virkkula, A., Gini, M., Eleftheriadis, K., Müller, T., Ohata, S., Kondo, Y., and Hyvärinen, A.: Characterizing the Arctic absorbing aerosol with multi-instrument observations, Atmos. Meas. Tech. Discuss., https://doi.org/10.5194/amt-2020-400, 2020.

Backman, J., Schmeisser, L., Virkkula, A., Ogren, J. A., Asmi, E., Starkweather, S., Sharma, S., Eleftheriadis, K., Uttal, T., Jefferson, A., Bergin, M., Makshtas, A., Tunved, P., and Fiebig, M.: On Aethalometer measurement uncertainties and an instrument correction factor for the Arctic, Atmos. Meas. Tech., 10, 5039–5062, https://doi.org/10.5194/amt-10-5039-2017, 2017.

Baumgardner, D., Popovicheva, O., Allan, J., Bernardoni, V., Cao, J., Cavalli, F., Cozic, J., Diapouli, E., Eleftheriadis, K., Genberg, P. J., Gonzalez, C., Gysel, M., John, A., Kirchstetter, T. W., Kuhlbusch, T. A. J., Laborde, M., Lack, D., Müller, T., Niessner, R., Petzold, A., Piazzalunga, A., Putaud, J. P., Schwarz, J., Sheridan, P., Subramanian, R., Swietlicki, E., Valli, G., Vecchi, R., and Viana, M.: Soot reference materials for instrument calibration and intercomparisons: A workshop summary with recommendations, Atmos. Meas. Tech., 5, 1869–1887, https://doi.org/10.5194/amt-5-1869-2012, 2012.

Bellouin, N., Quaas, J., Gryspeerdt, E., Kinne, S., Stier, P., Watson-Parris, D., Boucher, O., Carslaw, K. S., Christensen, M., Daniau, A.-L., Dufresne, J.-L., Feinglod, G., Fiedler, S., Foster, P., Gettelman, A., Haywood, J. M., Lohmann, U., Malavelle, F., Mauritsen, T., McCoy, D. T., Myhre, G., Mülmenstädt, J., Neubauer, D., Possner, A., Rugenstein, M., Sato, Y., Schulz, M., Schwartz, S. E., Sourdeval, O., Storelvmo, T., Toll, V., Winker, D., and Stevens, B.: Bounding global aerosol radiative forcing of climate change, Rev. Geophys., 58, e2019RG000660, https://doi.org/10.1029/2019RG000660, 2020.

Bergstrom, R. W.: Predictions of the spectral absorption and extinction coefficients of an urban air pollution aerosol model, Atmos. Environ., 6, 247–258, https://doi.org/10.1016/0004-6981(72)90083-2, 1972.

Bond, T. C. and Bergstrom, R. W.: Light absorption by carbonaceous particles: An investigative review, Aerosol Sci. Tech., 40, 1, 27–67, https://doi.org/10.1080/02786820500421521, 2006.

Bond, T. C., Anderson, T. L., and Campbell, D.: Calibration and Intercomparison of Filter-Based Measurements of Visible Light Absorption by Aerosols, Aerosol Sci. Tech., 30, 6, 582–600, https://doi.org/10.1080/027868299304435, 1999.

Bond, T. C., Habib, G., and Bergstrom, R. W.: Limitations in the enhancement of visible light absorption due to mixing state, J. Geophys. Res. Atmos., 111, D20211, https://doi.org/10.1029/2006JD007315, 2006.

Bond, T. C., Doherty, S. J., Fahey, D. W., Forster, P. M., Berntsen, T., Deangelo, B. J., Flanner, M. G., Ghan, S., Kärcher, B., Koch, D., Kinne, S., Kondo, Y., Quinn, P. K., Sarofim, M. C., Schultz, M. G., Schulz, M., Venkataraman, C., Zhang, H., Zhang, S., Bellouin, N., Guttikunda, S. K., Hopke, P. K., Jacobson, M. Z., Kaiser, J. W., Klimont, Z., Lohmann, U., Schwarz, J. P., Shindell, D., Storelvmo, T., Warren, S. G., and Zender, C. S.: Bounding the role of black carbon in the climate system: A scientific assessment, J. Geophys. Res. Atmos., 118, 1–173, https://doi.org/10.1002/jgrd.50171, 2013.

Cho, C., Schwarz, J. P., Perring, A. E., Lamb, K. D., Kondo, Y., Park, J., Park, D., Shim, K., Park, J., Park, R. J., Lee, M., Song, C., and Kim, S.: Science of the Total Environment Light-absorption enhancement of black carbon in the Asian out flow inferred from airborne SP2 and in-situ measurements during KORUS-AQ, Sci. Total Environ., 773, 145531, https://doi.org/10.1016/j.scitotenv.2021.145531, 2021.

Eleftheriadis, K., Vratolis, S., and Nyeki, S.: Aerosol black carbon in the European Arctic: Measurements at Zeppelin station, Ny-Ålesund, Svalbard from 1998–2007, Geophys. Res. Lett., 36, L02809, https://doi.org/10.1029/2008GL035741, 2009.

Eyring, V., Bony, S., Meehl, G. A., Senior, C. A., Stevens, B., Stouffer, R. J., and Taylor, K. E.: Overview of the Coupled Model Intercomparison Project Phase 6 (CMIP6) experimental design and organization, Geosci. Model Dev., 9, 1937–1958, https://doi.org/10.5194/gmd-9-1937-2016, 2016.

Flanner, M. G., Zender, C. S., Hess, P. G., Mahowald, N. M., Painter, T. H., Ramanathan, V., and Rasch, P. J.: Springtime warming and reduced snow cover from carbonaceous particles, Atmos. Chem. Phys., 9, 2481–2497, https://doi.org/10.5194/acp-9-2481-2009, 2009.

Gysel, M., Laborde, M., Olfert, J. S., Subramanian, R., and Gréhn, A. J.: Effective density of Aquadag and fullerene soot black carbon reference materials used for SP2 calibration, Atmos. Meas. Tech., 4, 2851–2858, https://doi.org/10.5194/amt-4-2851-2011, 2011.

Hansen, A. D. A., Rosen, H., and Novakov, T.: The aethalometer – an instrument for the real-time measurement of optical absorption by aerosol particles, Sci. Total Environ., 36, 191–196, 1984.

Huffman, D. R. and Stapp, J. L.: Optical Measurements on Solids of Possible Interstellar Importance, in: Interstellar dust and related topics, edited by: Greenberg, J. M. and Van de Hulst, H. C., Reidel, Boston, pp. 297–301, 1973.

Hyvärinen, A. P., Kolmonen, P., Kerminen, V. M., Virkkula, A., Leskinen, A., Komppula, M., Hatakka, J., Burkhart, J., Stohl, A., Aalto, P., Kulmala, M., Lehtinen, K. E. J., Viisanen, Y., and Lihavainen, H.: Aerosol black carbon at five background measurement sites over Finland, a gateway to the Arctic, Atmos. Environ., 45, 4042–4050, https://doi.org/10.1016/j.atmosenv.2011.04.026, 2011.

Irwin, M., Kondo, Y., and Moteki, N.: An empirical correction factor for filter-based photo-absorption black carbon measurements, J. Aerosol Sci., 80, 86–97, https://doi.org/10.1016/j.jaerosci.2014.11.001, 2015.

Kanaya, Y., Taketani, F., Komazaki, Y., Liu, X., Kondo, Y., Sahu, L. K., Irie, H., and Takashima, H.: Comparison of black carbon mass concentrations observed by multi-angle absorption photometer (MAAP) and continuous soot-monitoring system (COSMOS) on Fukue Island and in Tokyo, Japan, Aerosol Sci. Tech., 47, 1, 1–10, https://doi.org/10.1080/02786826.2012.716551, 2013.

Kanaya, Y., Pan, X., Miyakawa, T., Komazaki, Y., Taketani, F., Uno, I., and Kondo, Y.: Long-term observations of black carbon mass concentrations at Fukue Island, western Japan, during 2009–2015: constraining wet removal rates and emission strengths from East Asia, Atmos. Chem. Phys., 16, 10689–10705, https://doi.org/10.5194/acp-16-10689-2016, 2016.

Kanaya, Y., Yamaji, K., Miyakawa, T., Taketani, F., Zhu, C., Choi, Y., Komazaki, Y., Ikeda, K., Kondo, Y., and Klimont, Z.: Rapid reduction in black carbon emissions from China: Evidence from 2009-2019 observations on Fukue Island, Japan, Atmos. Chem. Phys., 20, 6339–6356, https://doi.org/10.5194/acp-20-6339-2020, 2020.

Kondo, Y.: Effects of Black Carbon on Climate: Advances in Measurement and Modeling, Monogr. Environ. Earth Planets, 3, 1–85, https://doi.org/10.5047/meep.2015.00301.0001, 2015.

Kondo, Y., Sahu, L., Kuwata, M., Miyazaki, Y., Takegawa, N., Moteki, N., Imaru, J., Han, S., Nakayama, T., Oanh, N. T. K., Hu, M., Kim, Y. J., and Kita, K.: Stabilization of the mass absorption cross section of black carbon for filter-based absorption photometry by the use of a heated inlet, Aerosol Sci. Tech., 43, 8, 741–756, https://doi.org/10.1080/02786820902889879, 2009.

Kondo, Y., Sahu, L., Moteki, N., Khan, F., Takegawa, N., Liu, X., Koike, M., and Miyakawa, T.: Consistency and traceability of black carbon measurements made by laser-induced incandescence, thermal-optical transmittance, and filter-based photo-absorption techniques, Aerosol Sci. Tech., 45, 2, 295–312, https://doi.org/10.1080/02786826.2010.533215, 2011.

Krecl, P., Ström, J., and Johansson, C.: Carbon content of atmospheric aerosols in a residential area during the wood combustion season in Sweden, Atmos. Environ., 41, 6974–6985, https://doi.org/10.1016/j.atmosenv.2007.06.025, 2007.

Laborde, M., Mertes, P., Zieger, P., Dommen, J., Baltensperger, U., and Gysel, M.: Sensitivity of the Single Particle Soot Photometer to different black carbon types, Atmos. Meas. Tech., 5, 1031–1043, https://doi.org/10.5194/amt-5-1031-2012, 2012.

Lack, D. A., Cappa, C. D., Covert, D. S., Baynard, T., Massoli, P., Sierau, B., Bates, T. S., Quinn, P. K., Lovejoy, E. R., and Ravishankara, A. R.: Bias in filter-based aerosol light absorption measurements due to organic aerosol loading: Evidence from ambient measurements, Aerosol. Sci. Tech., 42, 1033–1041, https://doi.org/10.1080/02786820802389277, 2008.

Lamb, K. D.: Classification of iron oxide aerosols by a single particle soot photometer using supervised machine learning, Atmos. Meas. Tech., 12, 3885–3906, https://doi.org/10.5194/amt-12-3885-2019, 2019.

Lihavainen, H., Hyvärinen, A., Asmi, E., Hatakka, J., and Viisanen, Y.: Long-term variability of aerosol optical properties in northern Finland, Boreal Env. Res., 20, 526–541, 2015.

Mason, B., Wagner, N. L., Adler, G., Andrews, E., Brock, C. A., Gordon, T. D., Lack, D. A., Perring, A. E., Richardson, M. S., Schwarz, J. P., Shook, M. A., Thornhill, K. L., Ziemba, L. D., and Murphy, D. M.: An intercomparison of aerosol absorption measurements conducted during the SEAC^{4}RS campaign, Aerosol Sci. Tech., 52, 1012–1027, https://doi.org/10.1080/02786826.2018.1500012, 2018.

Matsui, H., Mahowald, N. M., Moteki, N., Hamilton, D. S., Ohata, S., Yoshida, A., Koike, M., Scanza, R. A., and Flanner, M. G.: Anthropogenic combustion iron as a complex climate forcer, Nat. Commun., 9, https://doi.org/10.1038/s41467-018-03997-0, 2018.

Miyakawa, T., Oshima, N., Taketani, F., Komazaki, Y., Yoshino, A., Takami, A., Kondo, Y., and Kanaya, Y.: Alteration of the size distributions and mixing states of black carbon through transport in the boundary layer in east Asia, Atmos. Chem. Phys., 17, 5851–5864, https://doi.org/10.5194/acp-17-5851-2017, 2017.

Miyazaki, Y., Kondo, Y., Sahu, L. K., Imaru, J., Fukushima, N., and Kano, M.: Performance of a newly designed continuous soot monitoring system (COSMOS), J. Environ. Monitor., 10, 1195–1201, https://doi.org/10.1039/b806957c, 2008.

Moosmüller, H., Chakrabarty, R.K., and Arnott, W.P.: Aerosol light absorption and its measurement: A review, J. Quant. Spectrosc. Radiat. Transf., 110, 844–878, https://doi.org/10.1016/j.jqsrt.2009.02.035, 2009.

Moteki, N. and Kondo, Y.: Dependence of laser-induced incandescence on physical properties of black carbon aerosols: Measurements and theoretical interpretation, Aerosol Sci. Technol., 44, 8, 663–675, https://doi.org/10.1080/02786826.2010.484450, 2010.

Moteki, N., Adachi, K., Ohata, S., Yoshida, A., Harigaya, T., Koike, M., and Kondo, Y.: Anthropogenic iron oxide aerosols enhance atmospheric heating, Nat. Commun., 8, https://doi.org/10.1038/ncomms15329, 2017.

Müller, T., Henzing, J. S., De Leeuw, G., Wiedensohler, A., Alastuey, A., Angelov, H., Bizjak, M., Collaud Coen, M., Engström, J. E., Gruening, C., Hillamo, R., Hoffer, A., Imre, K., Ivanow, P., Jennings, G., Sun, J. Y., Kalivitis, N., Karlsson, H., Komppula, M., Laj, P., Li, S. M., Lunder, C., Marinoni, A., Martins Dos Santos, S., Moerman, M., Nowak, A., Ogren, J. A., Petzold, A., Pichon, J. M., Rodriquez, S., Sharma, S., Sheridan, P. J., Teinilä, K., Tuch, T., Viana, M., Virkkula, A., Weingartner, E., Wilhelm, R., and Wang, Y. Q.: Characterization and intercomparison of aerosol absorption photometers: result of two intercomparison workshops, Atmos. Meas. Tech., 4, 245–268, https://doi.org/10.5194/amt-4-245-2011, 2011.

Ogren, J. A.: Comment on “calibration and intercomparison of filter-based measurements of visible light absorption by aerosols,” Aerosol Sci. Tech., 44, 8, 589–591, https://doi.org/10.1080/02786826.2010.482111, 2010.

Ogren, J. A., Wendell, J., Andrews, E., and Sheridan, P. J.: Continuous light absorption photometer for long-term studies, Atmos. Meas. Tech., 10, 4805–4818, https://doi.org/10.5194/amt-10-4805-2017, 2017.

Ohata, S., Yoshida, A., Moteki, N., Adachi, K., Takahashi, Y., Kurisu, M., and Koike, M.: Abundance of Light-Absorbing Anthropogenic Iron Oxide Aerosols in the Urban Atmosphere and Their Emission Sources, J. Geophys. Res. Atmos., 123, 8115–8134, https://doi.org/10.1029/2018JD028363, 2018.

Ohata, S., Kondo, Y., Moteki, N., Mori, T., Yoshida, A., Sinha, P. R., and Koike, M.: Accuracy of black carbon measurements by a filter-based absorption photometer with a heated inlet, Aerosol Sci. Tech., 53, 9, 1079–1091, https://doi.org/10.1080/02786826.2019.1627283, 2019.

Oshima, N., Yukimoto, S., Deushi, M., Koshiro, T., Kawai, H., Tanaka, T. Y., and Yoshida, K.: Global and Arctic Radiative Forcing of Anthropogenic Gases and Aerosols in MRI-ESM2.0, Prog. Earth Planet. Sci., 7, 38, https://doi.org/10.1186/s40645-020-00348-w, 2020.

Petzold, A., Kramer, H., and Schönlinner, M.: Continuous measurement of atmospheric black carbon using a multi-angle absorption photometer, Environ. Sci. Pollut. R. Special issue 4, 78–82, 2002.

Petzold, A. and Schönlinner, M.: Multi-angle absorption photometry – A new method for the measurement of aerosol light absorption and atmospheric black carbon, J. Aerosol Sci., 35, 421–441, https://doi.org/10.1016/j.jaerosci.2003.09.005, 2004.

Petzold, A., Schloesser, H., Sheridan, P. J., Arnott, W. P., Ogren, J. A., and Virkkula, A.: Evaluation of multiangle absorption photometry for measuring aerosol light absorption, Aerosol Sci. Tech., 39, 1, 40–51, https://doi.org/10.1080/027868290901945, 2005.

Petzold, A., Ogren, J. A., Fiebig, M., Laj, P., Li, S. M., Baltensperger, U., Holzer-Popp, T., Kinne, S., Pappalardo, G., Sugimoto, N., Wehrli, C., Wiedensohler, A., and Zhang, X.-Y.: Recommendations for reporting black carbon measurements, Atmos. Chem. Phys., 13, 8365–8379, https://doi.org/10.5194/acp-13-8365-2013, 2013.

Pileci, R. E., Modini, R. L., Bertò, M., Yuan, J., Corbin, J. C., Marinoni, A., Henzing, B., Moerman, M. M., Putaud, J. P., Spindler, G., Wehner, B., Müller, T., Tuch, T., Trentini, A., Zanatta, M., Baltensperger, U., and Gysel-Beer, M.: Comparison of co-located refractory black carbon (rBC) and elemental carbon (EC) mass concentration measurements during field campaigns at several European sites, Atmos. Meas. Tech., 14, 1379–1403, https://doi.org/10.5194/amt-14-1379-2021, 2021.

Sand, M., Berntsen, T. K., Von Salzen, K., Flanner, M. G., Langner, J., and Victor, D. G.: Response of Arctic temperature to changes in emissions of short-lived climate forcers, Nat. Clim. Change, 6, 286–289, https://doi.org/10.1038/nclimate2880, 2016.

Schmeisser, L., Andrews, E., Ogren, J. A., Sheridan, P., Jefferson, A., Sharma, S., Kim, J. E., Sherman, J. P., Sorribas, M., Kalapov, I., Arsov, T., Angelov, C., Mayol-Bracero, O. L., Labuschagne, C., Kim, S.-W., Hoffer, A., Lin, N.-H., Chia, H.-P., Bergin, M., Sun, J., Liu, P., and Wu, H.: Classifying aerosol type using in situ surface spectral aerosol optical properties, Atmos. Chem. Phys., 17, 12097–12120, https://doi.org/10.5194/acp-17-12097-2017, 2017.

Schmeisser, L., Backman, J., Ogren, J. A., Andrews, E., Asmi, E., Starkweather, S., Uttal, T., Fiebig, M., Sharma, S., Eleftheriadis, K., Vratolis, S, Bergin, M., Tunved, P., and Jefferson, A.: Seasonality of aerosol optical properties in the Arctic, Atmos. Chem. Phys., 18, 11599–11622, https://doi.org/10.5194/acp-18-11599-2018, 2018.

Schmid, H., Laskus, L., Jürgen Abraham, H., Baltensperger, U., Lavanchy, V., Bizjak, M., Burba, P., Cachier, H., Crow, D., Chow, J., Gnauk, T., Even, A., Ten Brink, H. M., Giesen, K. P., Hitzenberger, R., Hueglin, C., Maenhaut, W., Pio, C., Carvalho, A., Putaud, J. P., Toom-Sauntry, D., and Puxbaum, H.: Results of the “carbon conference” international aerosol carbon round robin test stage I, Atmos. Environ., 35, 2111–2121, https://doi.org/10.1016/S1352-2310(00)00493-3, 2001.

Schulz, H., Zanatta, M., Bozem, H., Richard Leaitch, W., Herber, A. B., Burkart, J., Willis, M. D., Kunkel, D., Hoor, P. M., Abbatt, J. P. D., and Gerdes, R.: High Arctic aircraft measurements characterising black carbon vertical variability in spring and summer, Atmos. Chem. Phys., 19, 2361–2384, https://doi.org/10.5194/acp-19-2361-2019, 2019.

Schwarz, J. P., Gao, R. S., Fahey, D. W., Thomson, D. S., Watts, L. A., Wilson, J. C., Reeves, J. M., Darbeheshti, M., Baumgardner, D. G., Kok, G. L., Chung, S. H., Schulz, M., Hendricks, J., Lauer, A., Kärcher, B., Slowik, J. G., Rosenlof, K. H., Thompson, T. L., Langford, A. O., Loewenstein, M., and Aikin, K. C.: Single-particle measurements of midlatitude black carbon and light-scattering aerosols from the boundary layer to the lower stratosphere, J. Geophys. Res. Atmos., 111, D16207, https://doi.org/10.1029/2006JD007076, 2006.

Sharma, S., Lavoué, D., Chachier, H., Barrie, L. A. and Gong, S. L.: Long-term trends of the black carbon concentrations in the Canadian Arctic, J. Geophys. Res., 109, D15203, https://doi.org/10.1029/2003JD004331, 2004.

Sharma, S., Andrews, E., Barrie, L. A., Ogren, J. A., and Lavoué, D.: Variations and sources of the equivalent black carbon in the high Arctic revealed by long-term observations at Alert and

Barrow: 1989–2003, J. Geophys. Res., 111, D14028, https://doi.org/10.1029/2005JD006581, 2006.

Sharma, S., Leaitch, W. R., Huang, L., Veber, D., Kolonjari, F., Zhang, W., Hanna, S. J., Bertram, A. K., and Ogren, J. A.: An evaluation of three methods for measuring black carbon in Alert, Canada, Atmos. Chem. Phys., 17, 15225–15243, https://doi.org/10.5194/acp-17-15225-2017, 2017.

Sinha, P. R., Kondo, Y., Koike, M., Ogren, J. A., Jefferson, A., Barrett, T. E., Sheesley, R. J., Ohata, S., Moteki, N., Coe, H., Liu, D., Irwin, M., Tunved, P., Quinn, P. K., and Zhao, Y.: Evaluation of ground-based black carbon measurements by filter-based photometers at two Arctic sites, J. Geophys. Res. Atmos., 122, 3544–3572. https://doi.org/10.1002/2016JD025843, 2017.

World Meteorological Organization/Global Atmosphere Watch: WMO/GAW aerosol measurement procedures, guidelines, and recommendations, GAW Report No. 227, 2016.

Yoshida, A., Moteki, N., Ohata, S., Mori, T., Tada, R., Dagsson-Waldhauserová, P., and Kondo, Y.: Detection of light-absorbing iron oxide particles using a modified single-particle soot photometer, Aerosol Sci. Tech., 50, 3, i–iv, https://doi.org/10.1080/02786826.2016.1146402, 2016.

Yoshida, A., Ohata, S., Moteki, N., Adachi, K., Mori, T., Koike, M., and Takami, A.: Abundance and Emission Flux of the Anthropogenic Iron Oxide Aerosols From the East Asian Continental Outflow, J. Geophys. Res. Atmos., 123, 11, 194–11, 209, https://doi.org/10.1029/2018JD028665, 2018.

Yoshida, A., Moteki, N., Ohata, S., Mori, T., Koike, M., Kondo, Y., Matsui, H., Oshima, N., Takami, A., and Kita, K.: Abundances and Microphysical Properties of Light-Absorbing Iron Oxide and Black Carbon Aerosols Over East Asia and the Arctic, J. Geophys. Res. Atmos., 125, https://doi.org/10.1029/2019JD032301, 2020.

Yuan, J., Modini, R. L., Zanatta, M., Herber, A. B., Müller, T., Wehner, B., Poulain, L., Tuch, T., Baltensperger, U., and Gysel-beer, M.: Variability in the mass absorption cross section of black carbon (BC) aerosols is driven by BC internal mixing state at a central European background site (Melpitz, Germany) in winter, Atmos. Chem. Phys., 21, 635–655, https://doi.org/10.5194/acp-21-635-2021, 2021.

Zanatta, M., Gysel, M., Bukowiecki, N., Müller, T., Weingartner, E., Areskoug, H., Fiebig, M., Yttri, K. E., Mihalopoulos, N., Kouvarakis, G., Beddows, D., Harrison, R. M., Cavalli, F., Putaud, J. P., Spindler, G., Wiedensohler, A., Alastuey, A., Pandolfi, M., Sellegri, K., Swietlicki, E., Jaffrezo, J. L., Baltensperger, U., and Laj, P.: A European aerosol phenomenology-5: Climatology of black carbon optical properties at 9 regional background sites across Europe, Atmos. Environ., 145, 346–364, https://doi.org/10.1016/j.atmosenv.2016.09.035, 2016.

Zanatta, M., Laj, P., Gysel, M., Baltensperger, U., Vratolis, S., Eleftheriadis, K., Kondo, Y., Dubuisson, P., Winiarek, V., Kazadzis, S., Tunved, P., and Jacobi, H.-W.: Effects of mixing state on optical and radiative properties of black carbon in the European Arctic, Atmos. Chem. Phys., 18, 14037–14057, https://doi.org/10.5194/acp-18-14037-2018, 2018.

Figures

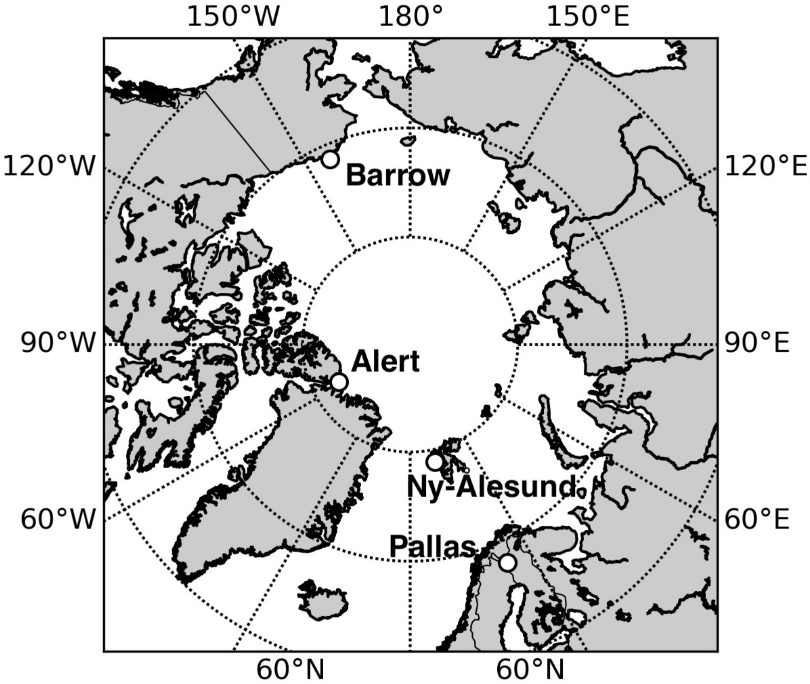

Figure 1. Locations of the Arctic sites where M_{BC} and b_{abs} were measured for this study.

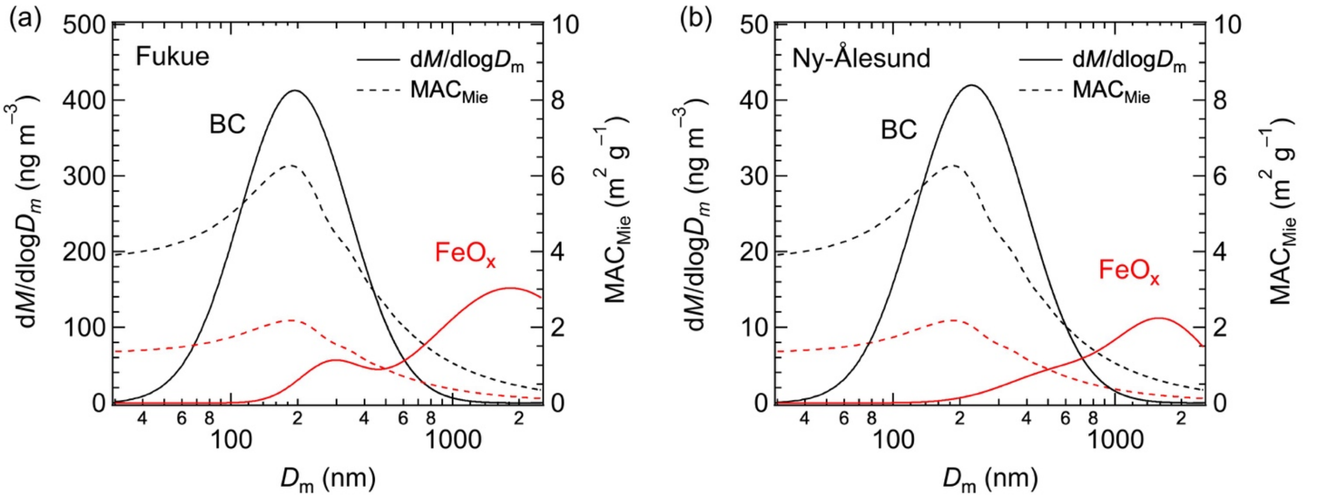

Figure 2. Mass size distributions of BC (black line) and FeO_x (red line) and mass absorption cross sections calculated by Mie theory for bare BC (black dashed line) and bare FeO_x (red dashed line) at (a) Fukue in April 2019 and (b) Ny-Ålesund in March 2017. D_m is the mass equivalent diameter of bare BC or FeO_x. Assumptions for the Mie calculations are given in Sect. 2.

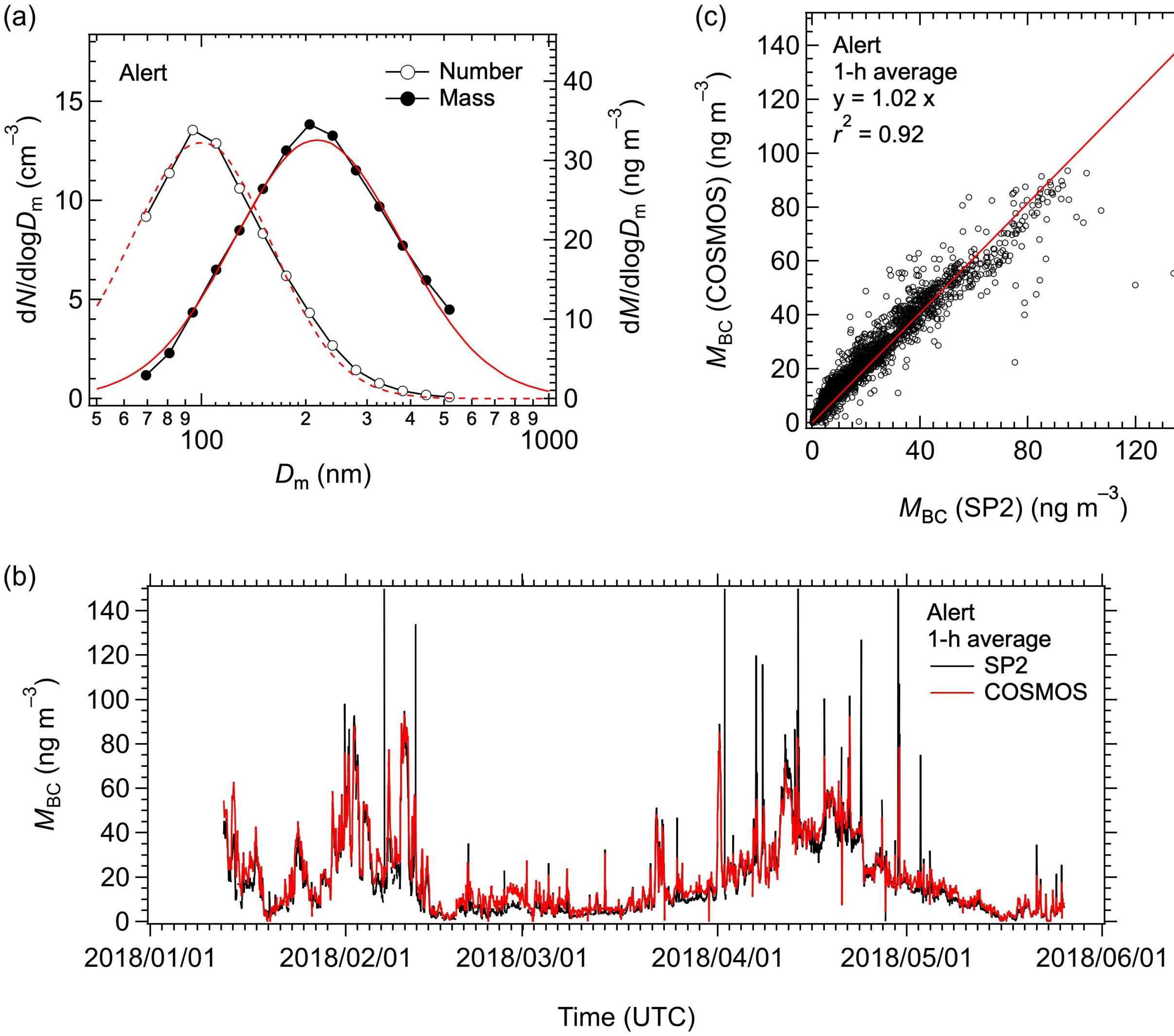

Figure 3. (a) Number and mass size distributions of BC averaged over the observation period at Alert from January to May 2018. The dashed (solid) red line is the lognormal fit to the number (mass) size distribution. (b) Time series (1-h data) and (c) correlation of M_{BC} measured by COSMOS and SP2. The solid red line in the correlation plot is the least squares regression forced through the origin.

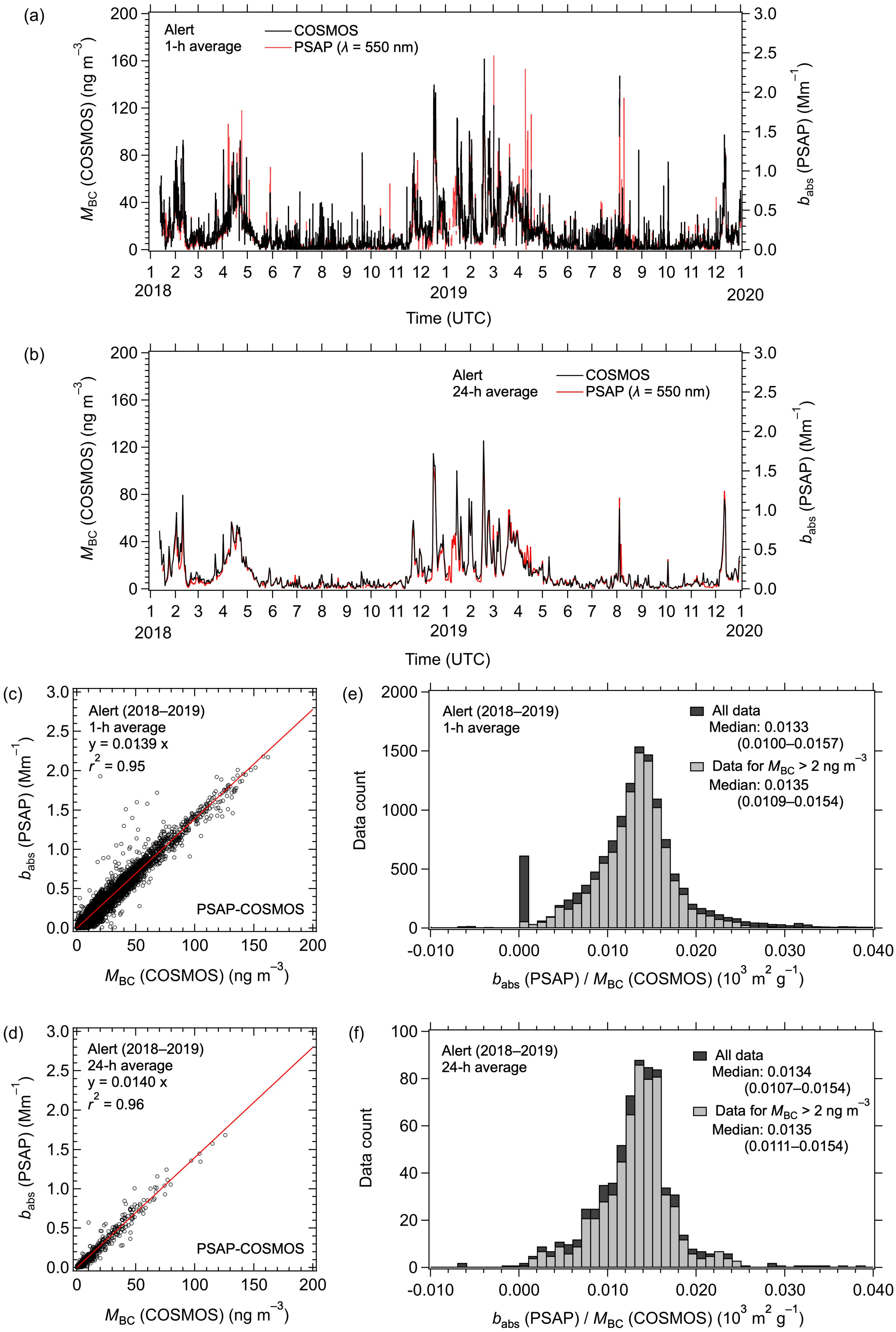

Figure 4. Time series of M_{BC} (COSMOS) and b_{abs} (PSAP; $\lambda = 550$ nm) from January 2018 to December 2019 at Alert for (a) 1-h averaged and (b) 24-h averaged data. (c) and (d) Corresponding correlations of M_{BC} (COSMOS) and b_{abs} (PSAP). The solid red lines are the least squares regressions forced through the origin. (e) and (f) Corresponding histograms of b_{abs} (PSAP) / M_{BC} (COSMOS) ratios for all data and data with M_{BC} (COSMOS) > 2 ng m^{-3}. The interquartile ranges are shown in parentheses.

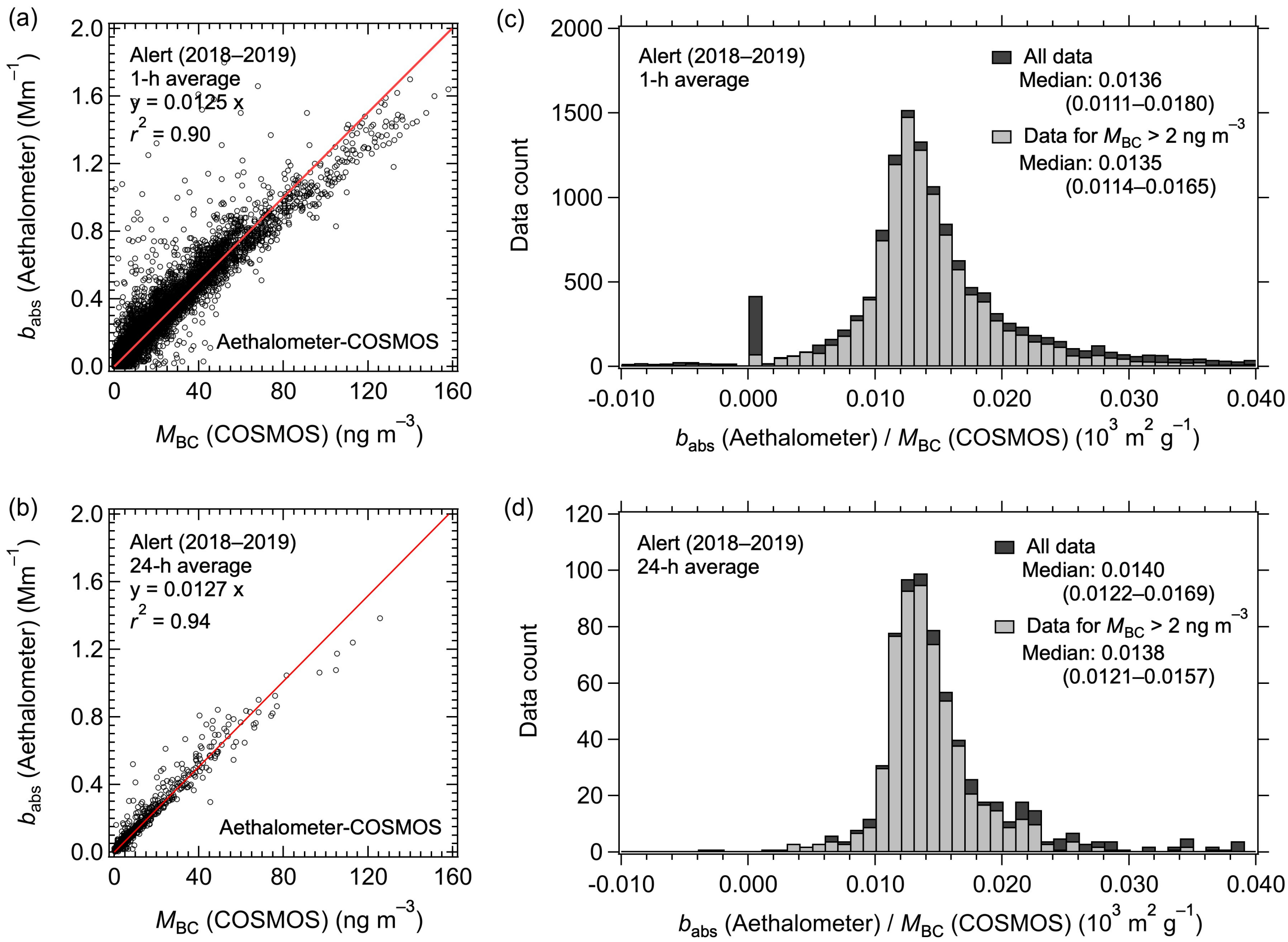

Figure 5. Correlations of M_{BC} (COSMOS) and b_{abs} (Aethalometer; λ = 590 nm) from January 2018 to December 2019 at Alert for (a) 1-h averaged and (b) 24-h averaged data. The solid red lines are the least squares regressions forced through the origin. (c) and (d) Corresponding histograms of b_{abs} (Aethalometer) / M_{BC} (COSMOS) ratios for all data and data with M_{BC} (COSMOS) > 2 ng m^{-3}.

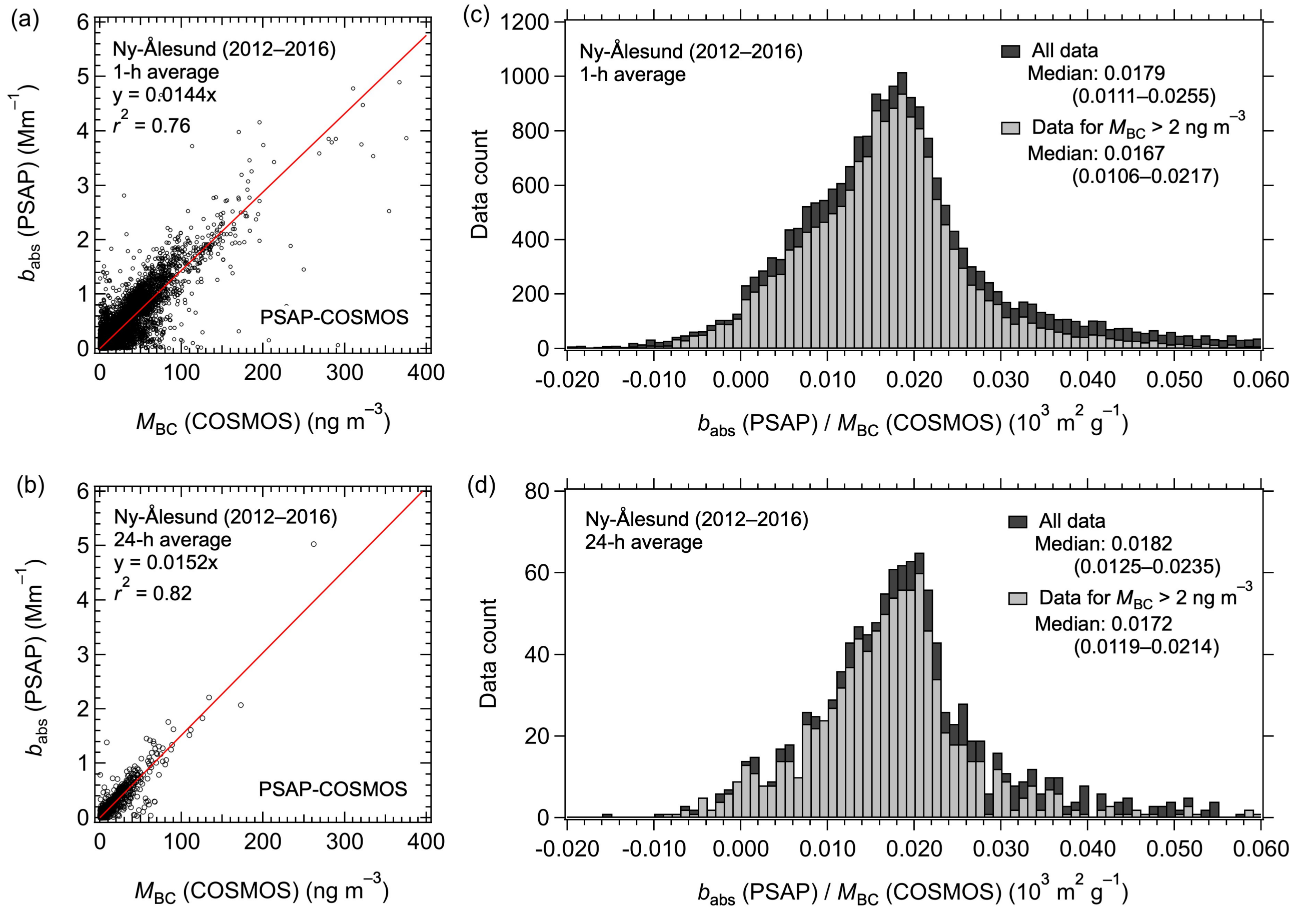

Figure 6. Correlations of M_{BC} (COSMOS) and b_{abs} (PSAP; $\lambda = 550$ nm) from April 2012 to September 2016 at Ny-Ålesund for (a) 1-h averaged and (b) 24-h averaged data. The solid red lines are the least squares regressions forced through the origin. (c) and (d) Corresponding histograms of b_{abs} (PSAP) / M_{BC} (COSMOS) ratios for all data and data with M_{BC} (COSMOS) > 2 ng m^{-3}.

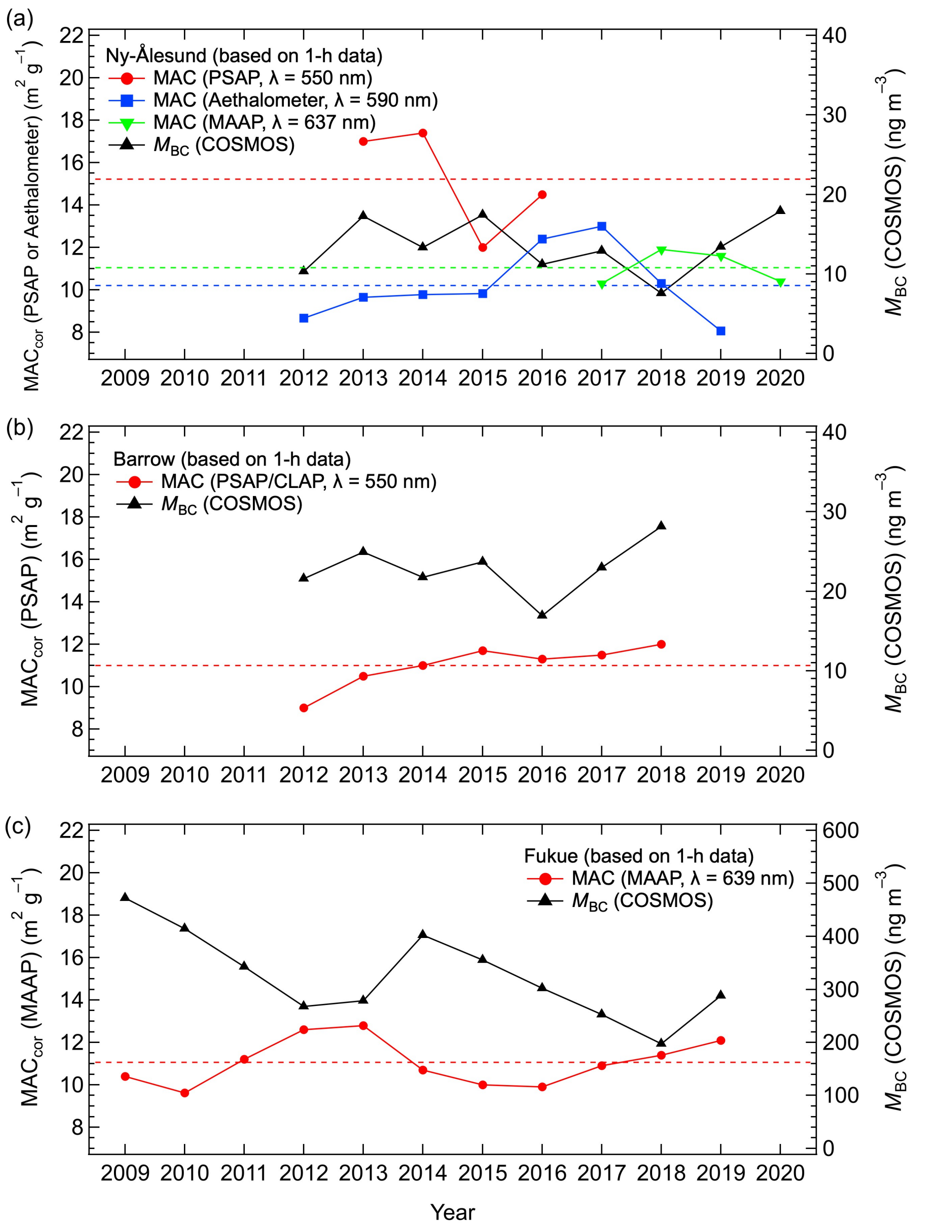

Figure 7. (a) Time series of yearly MAC_{cor} (PSAP; λ = 550 nm), MAC_{cor} (Aethalometer; λ = 590 nm), MAC_{cor} (MAAP; λ = 637 nm), and M_{BC} (COSMOS) at Ny-Ålesund. (b) Time series of yearly MAC_{cor} (PSAP/CLAP; λ = 550 nm) and M_{BC} (COSMOS) at Barrow. (c) Time series of yearly MAC_{cor} (MAAP; λ = 639 nm) and M_{BC} (COSMOS) at Fukue. In each panel, yearly MAC_{cor} and M_{BC} (COSMOS) are calculated from 1-h data. The dashed lines show the averages of yearly MAC_{cor} for the entire time series.

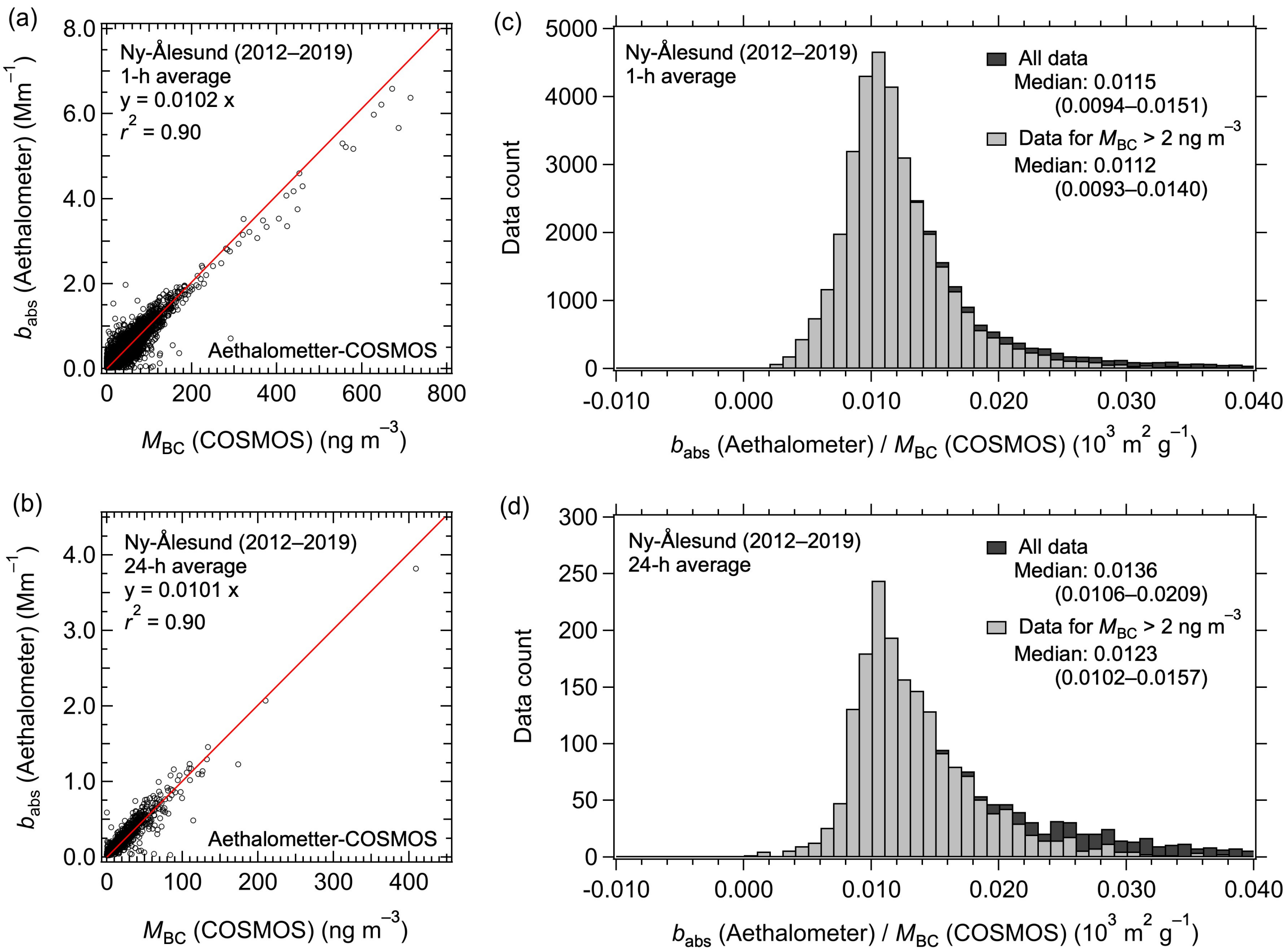

Figure 8. Correlations of M_{BC} (COSMOS) and b_{abs} (Aethalometer; λ = 590 nm) from April 2012 to August 2019 at Ny-Ålesund for (a) 1-h averaged and (b) 24-h averaged data. The solid red lines are the least squares regressions forced through the origin. (c) and (d) Corresponding histograms of b_{abs} (Aethalometer) / M_{BC} (COSMOS) ratios for all data and data with M_{BC} (COSMOS) > 2 ng m^{-3}.

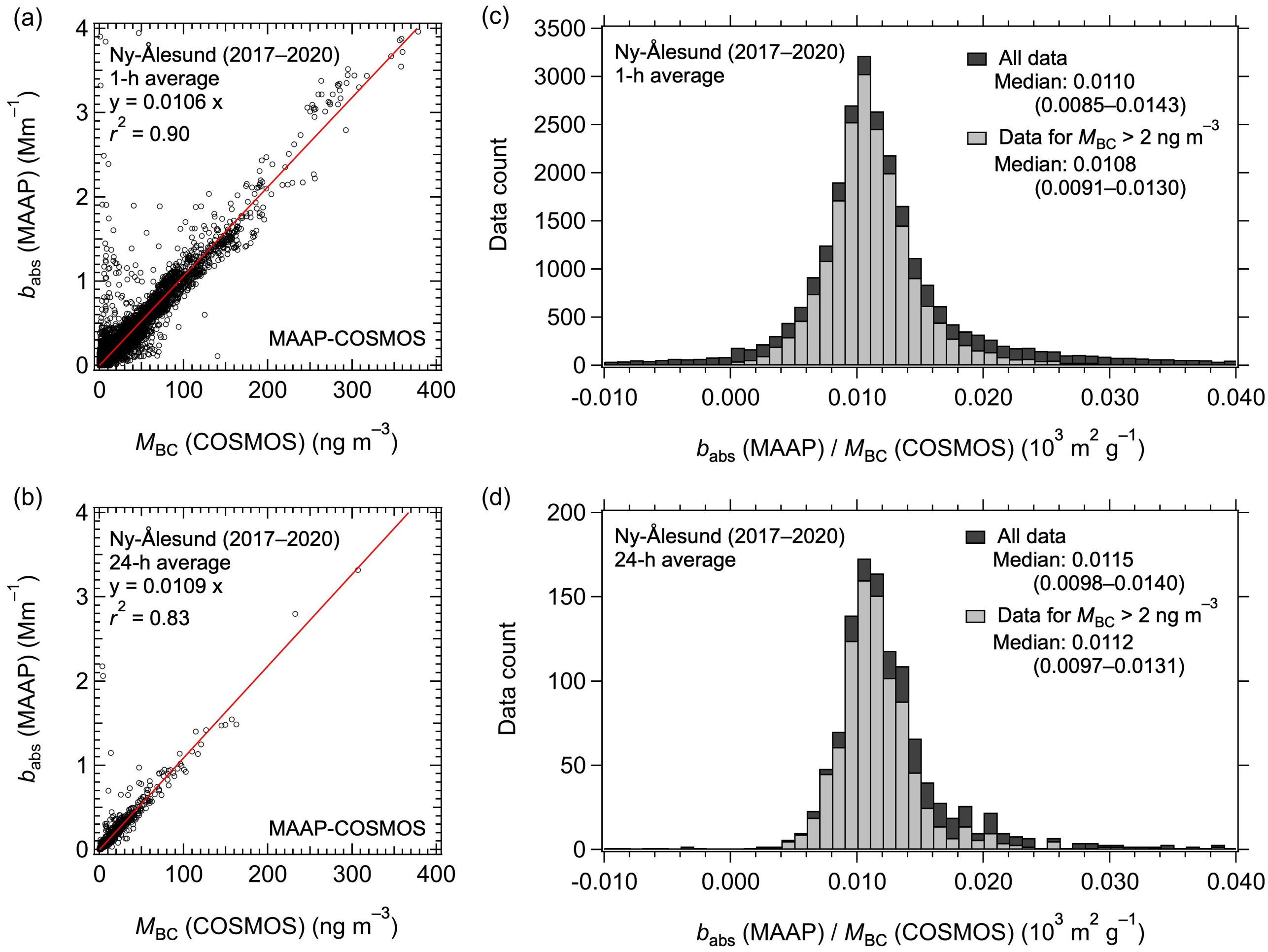

Figure 9. Correlations of M_{BC} (COSMOS) and b_{abs} (MAAP; λ = 637 nm) from January 2017 to December 2020 at Ny-Ålesund for (a) 1-h averaged and (b) 24-h averaged data. The solid red lines are the least squares regressions forced through the origin. (c) and (d) Corresponding histograms of b_{abs} (MAAP) / M_{BC} (COSMOS) ratios for all data and data with M_{BC} (COSMOS) > 2 ng m^{-3}.

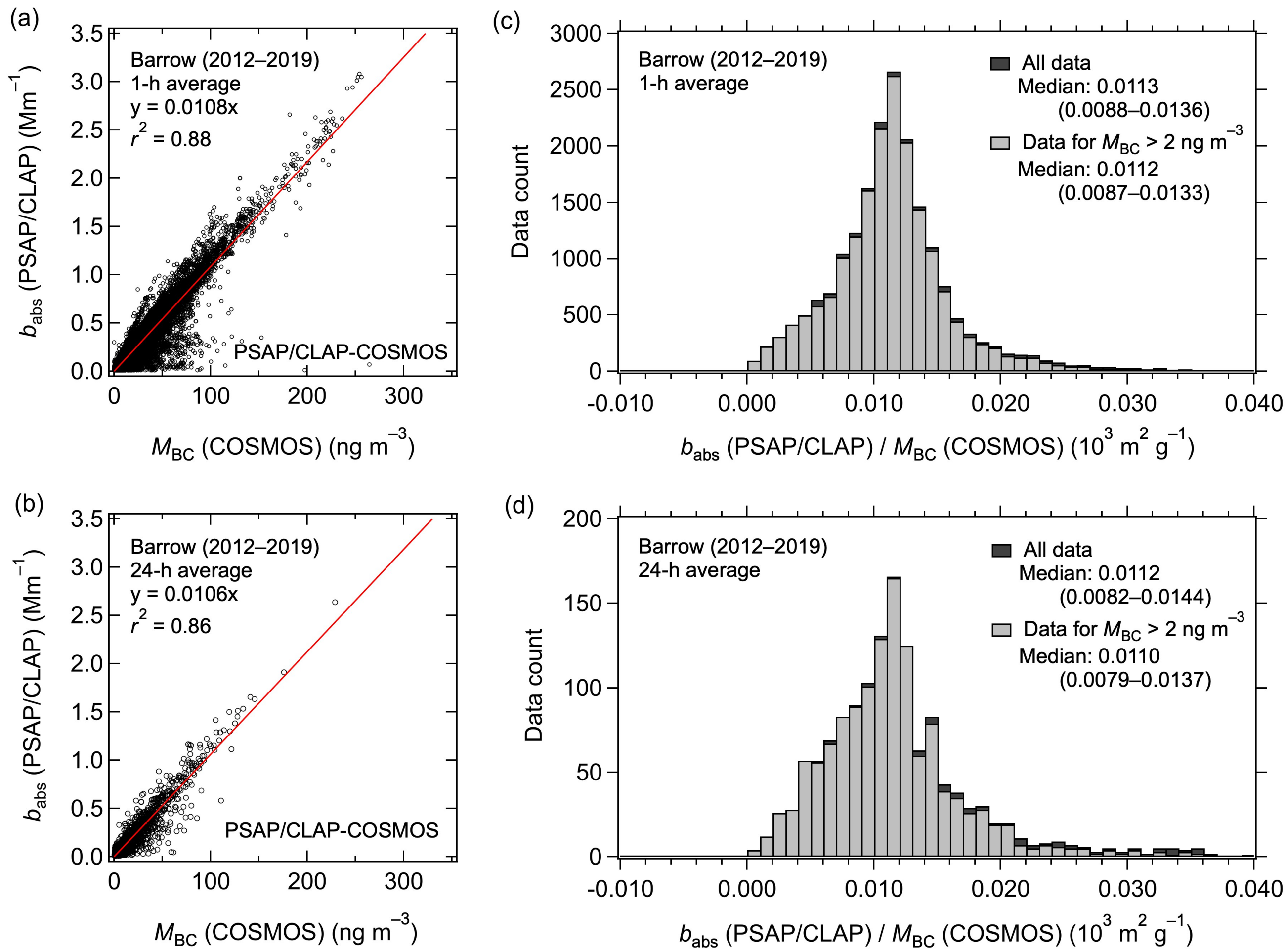

Figure 10. Correlations of M_{BC} (COSMOS) and b_{abs} (PSAP/CLAP; λ = 550 nm) from August 2012 to December 2019 at Barrow for (a) 1-h averaged and (b) 24-h averaged data. The solid red lines are the least squares regressions forced through the origin. (c) and (d) Corresponding histograms of b_{abs} (PSAP/CLAP) / M_{BC} (COSMOS) ratios for all data and data with M_{BC} (COSMOS) > 2 ng m^{-3}.

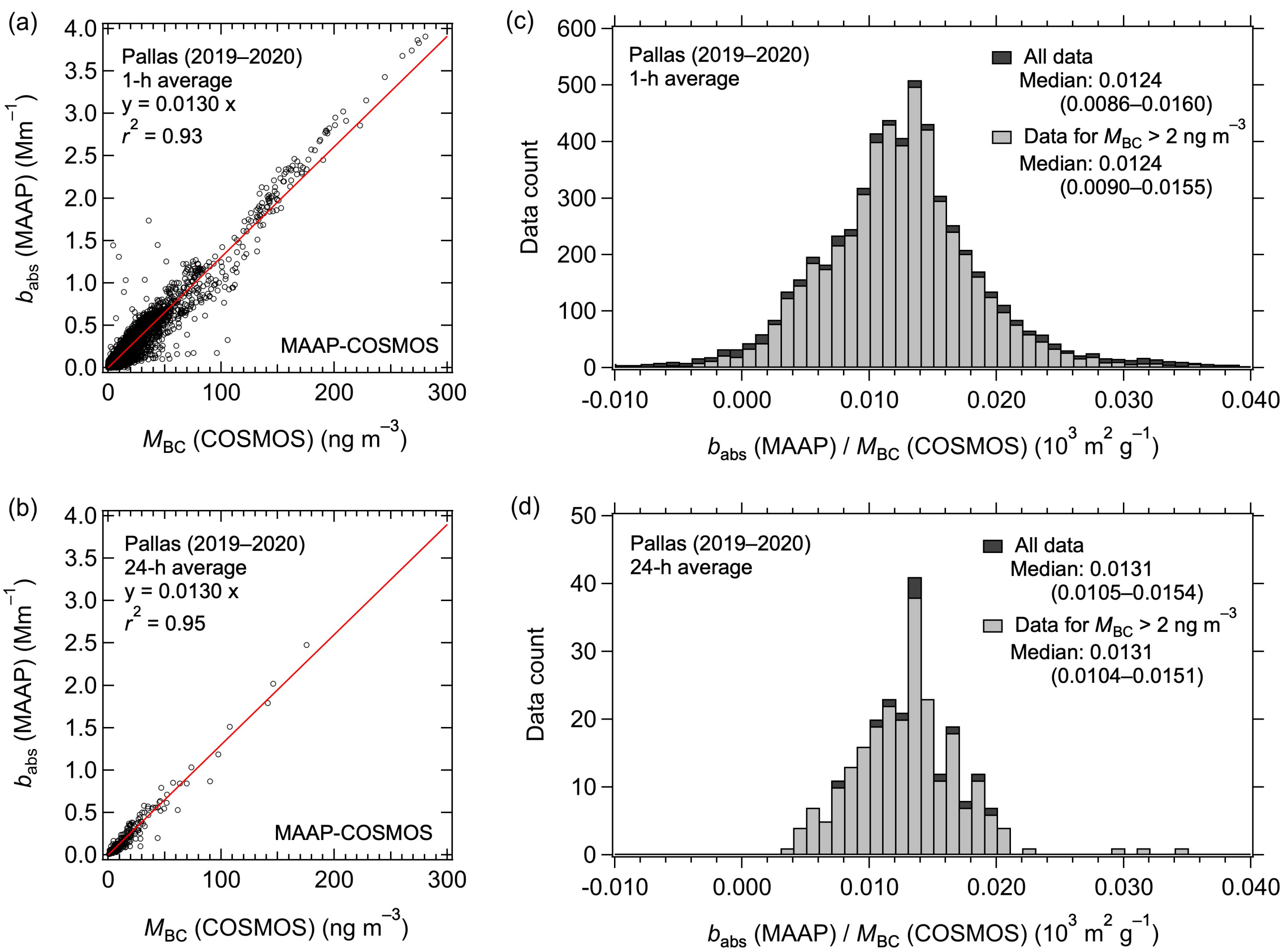

Figure 11. Correlations of M_{BC} (COSMOS) and b_{abs} (MAAP; λ = 637 nm) from July 2019 to July 2020 at Pallas for (a) 1-h averaged and (b) 24-h averaged data. The solid red lines are the least squares regressions forced through the origin. (c) and (d) Corresponding histograms of b_{abs} (MAAP) / M_{BC} (COSMOS) ratios for all data and data with M_{BC} (COSMOS) > 2 ng m^{-3}.

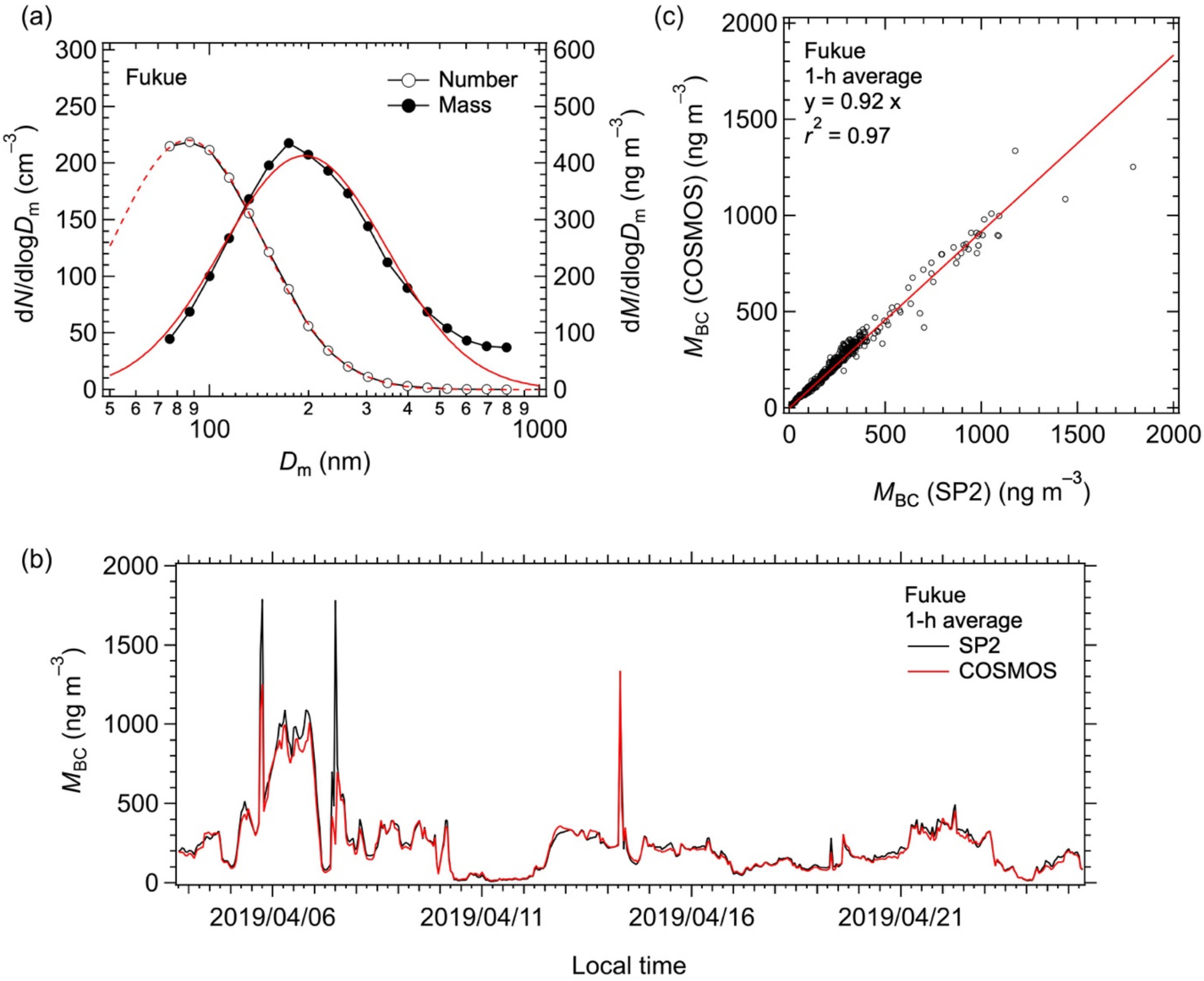

Figure 12. (a) Number and mass size distributions of BC averaged over the observation period at Fukue in April 2019. The dashed (solid) red line is the lognormal fit to the number (mass) size distribution. (b) Time series (1-h data) and (c) correlation of M_{BC} measured by COSMOS and SP2. The solid red line in the correlation plot is the least squares regression forced through the origin.

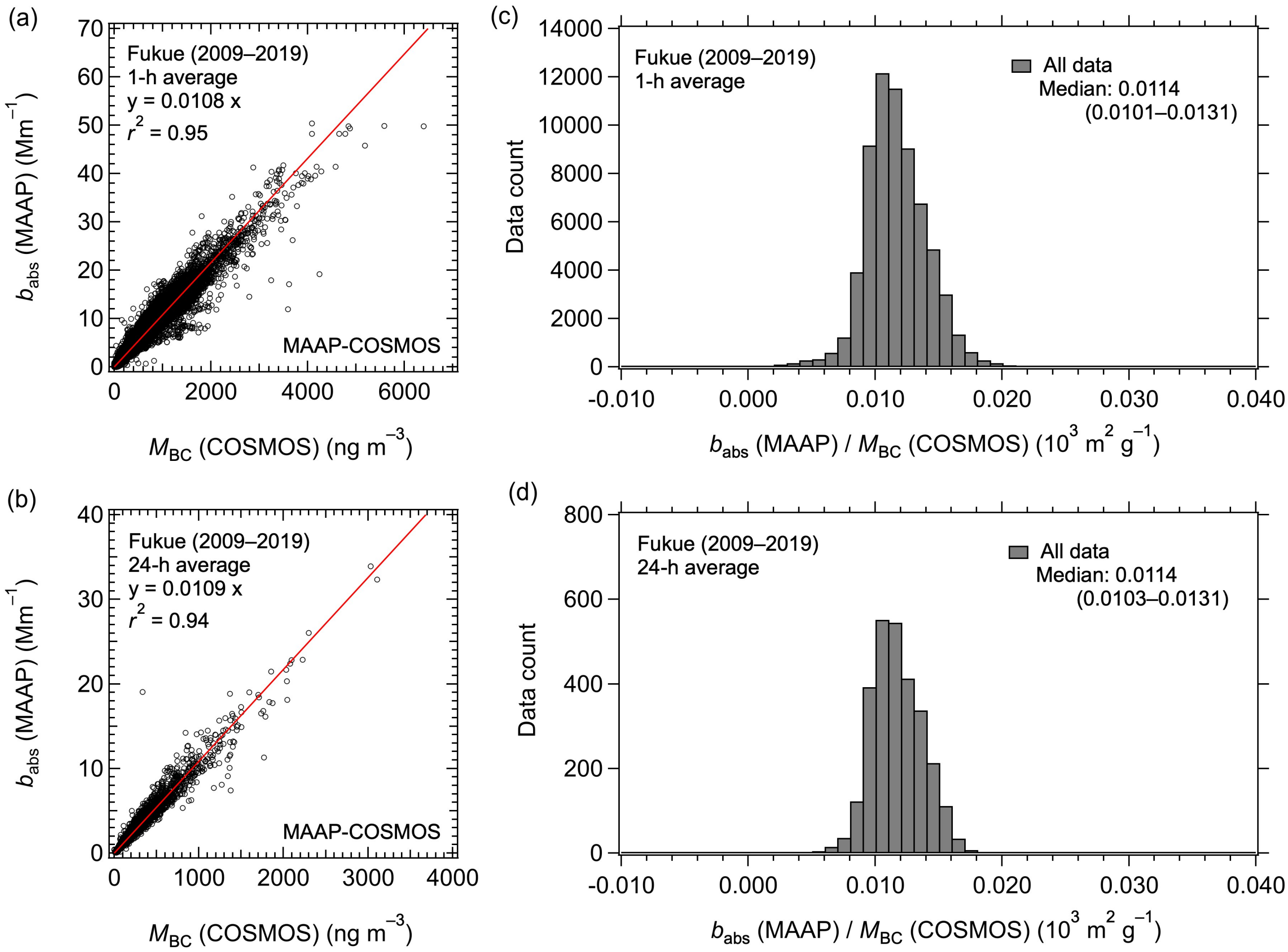

Figure 13. Correlations of M_{BC} (COSMOS) and b_{abs} (MAAP; λ = 639 nm) from April 2009 to May 2019 at Fukue for (a) 1-h averaged and (b) 24-h averaged data. The solid red lines are the least squares regression forced through the origin. (c) and (d) Corresponding histograms of b_{abs} (MAAP) / M_{BC} (COSMOS) ratios.

Tables

Table 1. Observation sites, periods, and instruments used in this study.

Location	Period	Instruments
Alert (ALT)	Jan – May 2018	COSMOS, EC-SP2
	Jan 2018 – Dec 2019	COSMOS, PSAP, Aethalometer (AE31)
Ny-Ålesund (ZEP)	Apr 2012 – Sep 2016	COSMOS, PSAP
	Apr 2012 – Aug 2019	COSMOS, Aethalometer (AE31)
	Jan 2017 – Dec 2020	COSMOS, MAAP
Barrow (BRW)	Aug 2012 – Dec 2019	COSMOS, PSAP, CLAP
Pallas (PAL)	Jul 2019 – Jul 2020	COSMOS, MAAP
Fukue (Japan) (FKE)	Apr 2019	COSMOS, UT-SP2
	Apr 2009 – May 2019	COSMOS, MAAP

Table 2. MAC_{cor} (PSAP/CLAP; λ) values at Alert during 2018–2019. r^2 is the square of the correlation coefficient.

Instrument	λ (nm)	MAC_{cor} (1-h) [m^2 g^{-1}]	r^2(1-h)	MAC_{cor} (24-h) [m^2 g^{-1}]	r^2 (24-h)
CLAP1	450	13.6	0.93	13.6	0.95
CLAP2	450	15.4	0.96	15.4	0.96
PSAP	450	15.7	0.95	15.4	0.96
CLAP1	550	12.1	0.93	12.1	0.95
CLAP2	550	13.6	0.96	13.8	0.95
PSAP	550	13.9	0.96	14.0	0.95
CLAP1	700	9.7	0.93	9.7	0.95
CLAP2	700	10.8	0.95	10.9	0.95
PSAP	700	11.5	0.94	11.6	0.95

Table 3. MAC, r^2, and variability of MAC (V_{MAC}; interquartile range in relative terms) of MAAP, PSAP/CLAP, and Aethalometer at observation sites in this study.

Site	Instrument	λ [nm]	Inlet	Period	(1-h) MAC_{cor} [$m^2\ g^{-1}$]	r^2	MAC_{med} [$m^2\ g^{-1}$]	V_{MAC} [%]	(24-h) MAC_{cor} [$m^2\ g^{-1}$]	r^2	MAC_{med} [$m^2\ g^{-1}$]	V_{MAC} [%]
ALT	PSAP	550	PM_1	2018–2019	13.9	0.95	13.5	19	14.0	0.96	13.5	18
ALT	AE31	590	TSP*	2018–2019	12.5	0.90	13.5	22	12.7	0.94	13.8	22
ZEP	PSAP	550	PM_{10}	2012–2016	14.4	0.76	16.7	37	15.2	0.82	17.2	31
ZEP	AE31	590	PM_{10}	2012–2019	10.2	0.90	11.2	25	10.1	0.90	12.3	28
ZEP	MAAP	637	TSP*	2017–2020	10.6	0.90	10.8	20	10.9	0.83	11.2	17
BRW	PSAP/CLAP	550	PM_1	2012–2019	10.8	0.88	11.2	22	10.6	0.86	11.0	26
PAL	MAAP	637	PM_{10}	2019–2020	13.0	0.93	12.4	27	13.0	0.95	13.1	21
FKE	MAAP	639	PM_1**	2009–2019	10.8	0.95	11.4	15	10.9	0.94	11.4	15

*Total suspended particle.
**A PM2.5 cyclone was used before November 2011.

Table 4. MAC_{cor} (Aethalometer; λ) and r^2 values at Alert during 2018–2019.

λ (nm)	MAC_{cor} (1-h) [$m^2\ g^{-1}$]	r^2(1-h)	MAC_{cor} (24-h) [$m^2\ g^{-1}$]	r^2 (24-h)
370	18.6	0.86	18.7	0.90
470	15.4	0.89	15.6	0.93
520	13.9	0.90	14.1	0.94
590	12.5	0.90	12.7	0.94
660	11.4	0.89	11.6	0.94
880	8.8	0.82	8.9	0.94
950	8.1	0.79	8.1	0.94

Table 5. MAC_{cor} (PSAP) and MAC_{cor} (Aethalometer) values derived from 24-h averaged data at Alert during 2018–2019.

λ (nm) PSAP/Aeth	MAC_{cor} (PSAP) [m^2 g^{-1}]	MAC_{cor} (Aeth) [m^2 g^{-1}]	MAC_{cor} (Aeth)/ MAC_{cor} (PSAP)
450/470	15.4	15.6	1.01 (1.06)[*]
550/590	14.0	12.7	1.01 (1.03)[*]
700/660	11.6	11.6	1.00 (0.94)[*]

[*] MAC_{cor} (Aethalometer) values measured at λ = 470, 590, and 660 nm were adjusted to those at λ = 450, 550, and 700 nm (wavelengths used for PSAP) by assuming an absorption Ångstrom exponent of 1.0.

Table 6. Year-to-year variability of MAC_{cor} (PSAP; λ = 550 nm) and r^2 at Ny-Ålesund.

Year	MAC_{cor} (1-h) [m^2 g^{-1}]	r^2 (1-h)	MAC_{cor} (24-h) [m^2 g^{-1}]	r^2 (24-h)
2012 (Apr–Dec)	5.7	0.30	5.8	0.44
2013	17.0	0.81	17.2	0.85
2014	17.4	0.80	18.5	0.81
2015	12.0	0.84	15.9	0.94
2016 (Jan–Sep)	14.5	0.90	14.8	0.95
Average (2013–2016)[*]	15.2 ± 2.2	0.84 ± 0.04	16.6 ± 1.4	0.89 ± 0.06
All[**]	14.4	0.76	15.2	0.82

[*]Average and standard deviation for individual years
[**]Derived by regression slope for all data points

Table 7. Year-to-year variability of MAC_{cor} (Aethalometer; λ = 590 nm) and r^2 at Ny-Ålesund.

Year	MAC_{cor} (1-h) [m^2 g^{-1}]	r^2 (1-h)	MAC_{cor} (24-h) [m^2 g^{-1}]	r^2 (24-h)
2012 (Apr–Dec)	8.67	0.80	8.75	0.85
2013	9.65	0.87	8.89	0.75
2014	9.77	0.92	10.0	0.95
2015	9.82	0.96	9.87	0.98
2016	12.4	0.92	12.2	0.95
2017	13.0	0.86	11.5	0.87
2018	10.3	0.92	10.6	0.94
2019 (Jan–Aug)	8.07	0.91	8.37	0.92
Average[*]	10.2 ± 1.6	0.90 ± 0.05	10.0 ± 1.3	0.90 ± 0.07
All[**]	10.2	0.90	10.1	0.90

[*]Average and standard deviation for individual years
[**]Derived by regression slope for of all data points

Table 8. Year-to-year variability of MAC_{cor} (MAAP; λ = 637 nm) and r^2 at Ny-Ålesund.

Year	MAC_{cor} (1-h) [m^2 g^{-1}]	r^2 (1-h)	MAC_{cor} (24-h) [m^2 g^{-1}]	r^2 (24-h)
2017	10.3	0.85	10.7	0.57
2018	11.9	0.74	13.3	0.64
2019	11.6	0.92	12.2	0.92
2020	10.4	0.92	10.5	0.97
Average*	11.1 ± 0.7	0.86 ± 0.07	11.7 ± 1.1	0.78 ± 0.17
All**	10.6	0.90	10.9	0.83

*Average and standard deviation for individual years
**Derived by regression slope for of all data points

Table 9. Year-to-year variability of MAC_{cor} (PSAP/CLAP; λ = 550 nm) and r^2 at Barrow.

Year	MAC_{cor} (1-h) [m^2 g^{-1}]	r^2 (1-h)	MAC_{cor} (24-h) [m^2 g^{-1}]	r^2 (24-h)
2012 (Aug–Dec)	9.00	0.65	8.80	0.67
2013	10.5	0.91	10.5	0.91
2014	11.0	0.96	10.8	0.91
2015	11.7	0.91	11.5	0.91
2016	11.3	0.89	11.2	0.88
2017	11.5	0.91	11.3	0.93
2018 (Jan–May)	12.0	0.86	10.9	0.69
2019 (Jun–Dec)	4.6	0.28	5.1	0.41
Average (2012–2018)*	11.0 ± 0.9	0.87 ± 0.09	10.7 ± 0.8	0.84 ± 0.10
All**	10.8	0.88	10.6	0.86

*Average and standard deviation for individual years
**Derived by regression slope for all data points

Table 10. Year-to-year variability of MAC_{cor} (MAAP; λ = 639 nm) and r^2 at Fukue.

Year	MAC_{cor} (1-h) [$m^2\ g^{-1}$]	r^2 (1-h)	MAC_{cor} (24-h) [$m^2\ g^{-1}$]	r^2 (24-h)
2009 (Apr–Dec)	10.4	0.98	10.5	0.99
2010	9.62	0.95	9.74	0.95
2011	11.2	0.95	11.3	0.96
2012	12.6	0.96	12.7	0.96
2013	12.8	0.94	12.7	0.94
2014	10.7	0.98	10.8	0.98
2015	10.0	0.96	9.96	0.95
2016	9.90	0.95	9.97	0.95
2017	10.9	0.93	11.1	0.90
2018	11.4	0.96	11.5	0.96
2019 (Jan–May)	12.1	0.95	12.2	0.95
Average*	11.1 ± 1.0	0.96 ± 0.01	11.1 ± 1.0	0.95 ± 0.02
All**	10.8	0.95	10.9	0.94

*Average and standard deviation for individual years
**Derived by regression slope for all data points

Table 11. MAC_{cor} and r^2 for MAAP, PSAP/CLAP, and Aethalometer at λ = 550 nm at observation sites in this study.

Site	Instrument	Inlet	Period	(1-h) MAC_{cor} [$m^2\ g^{-1}$]	r^2	(24-h) MAC_{cor} [$m^2\ g^{-1}$]	r^2
ALT	PSAP	PM_1	2018–2019	13.9	0.95	14.0	0.96
ALT	AE31	TSP*	2018–2019	13.4***	0.89	13.6***	0.92
ZEP	PSAP	PM_{10}	2013–2016	14.4	0.76	15.2	0.82
ZEP	AE31	PM_{10}	2012–2019	10.9***	0.90	10.8***	0.90
ZEP	MAAP	TSP*	2017–2020	12.3***	0.90	12.6***	0.83
BRW	PSAP/CLAP	PM_1	2012–2018	10.8	0.88	10.6	0.86
PAL	MAAP	PM_{10}	2019–2020	15.1***	0.93	15.1***	0.95
FKE	MAAP	PM_1**	2009–2019	12.5***	0.95	12.7***	0.95
Average for the 4 Arctic sites****				13.0±1.6	0.89±0.06	13.1±1.7	0.89±0.05

*Total suspended particles.
**A PM2.5 cyclone was used before November 2011.
*** MAC_{cor} (MAAP; λ ~637 nm) and MAC_{cor} (Aethalometer; λ = 590 nm) values were adjusted to λ = 550 nm by assuming an absorption Ångstrom exponent of 1.0.
****Average and standard deviation values were calculated excluding MAAP data at Fukue.